

Supporting Online Material

A Metastable Brominated Nanodiamond Surface Enables Room Temperature and Catalysis-free Amine Chemistry

Cynthia Melendrez^{Ψ,ξ}, Jorge A. Lopez-Rosas^{Ψ,ξ}, Camron X. Stokes^{Ψ,ξ}, Tsz Ching Cheung^Ψ, Sang-Jun Lee^Δ, Charles James Titus^{Δ,Φ}, Jocelyn Valenzuela,^Ψ Grace Jeanpierre^Ψ, Halim Muhammad^Ψ, Polo Tran^Ψ, Perla Jasmine Sandoval^Ψ, Tyanna Supreme^Ψ, Virginia Altoe^π, Jan Vavra^Ω, Helena Raabova^Ω, Vaclav Vanek^Ω, Sami Sainio^{Δ,λ}, William B. Doriese^Σ, Galen C. O'Neil^Σ, Daniel S. Swetz^Σ, Joel N. Ullom^Σ, Kent Irwin^{Δ,Φ}, Dennis Nordlund^Δ, Petr Cigler^Ω & Abraham Wolcott^{Ψ,*}

^Ψ Department of Chemistry
San José State University
San José, CA 95192

^πThe Molecular Foundry
Lawrence Berkeley National Laboratory
1 Cyclotron Road Berkeley, CA 94720

^ΩInstitute of Organic Chemistry and Biochemistry
Academy of Sciences of the Czech Republic
Flemingovo nam. 2, 166 10 Prague 6, Czech Republic

^Δ Stanford Synchrotron Radiation Lightsource
SLAC National Accelerator Laboratory
Menlo Park, CA 94025

^ΦStanford University
Department of Physics
Palo Alto, CA 94025

^λ University of Oulu
Microelectronics Research Unit
Faculty of Information Technology and Electrical
Engineering
Oulu, Finland

^ΣQuantum Electromagnetics Division
National Institute of Standards and Technology
Boulder, CO 80305

* Corresponding authors: A. Wolcott (abraham.wolcott@sjsu.edu)

ξ C.M., J.A.L-P and C.X.S. contributed equally

Table of Contents

1.	Materials and Procedures	page S3-10
2.	Time dependent study of bromination chemistry	page S11-13
3.	Debromination and analysis of ND-Br in open air and inert conditions	page S14-18
4.	Nanodiamond surface analysis based on XPS Survey Scans.	page S19-26
5.	N1s XAS Control Samples, X-ray beam damage and Amide Bond Formation using sulfo-NHS/EDC Coupling	page S26-27
6.	Suppression of the diamond electronic structure after ND-Br and propargylamine Sonogashira-type reaction	page S28-30
7.	Representative Carbon, Nitrogen and Oxygen RIXS Maps of aminated ND-Br samples	page S31-36
8.	Percent Reflectance and Normalized Reflectance of DRIFTS spectra from Figure 1.	page S37-38
9.	References	page S39-40

Materials and Procedures

Materials. High-pressure high-temperature nanodiamond powders (monocrystalline diamond powder, MSY 0-0.03 micron and MSY 0-0.05 micron) were purchased from Microdiamant, USA. Anhydrous dichloromethane (99.8% #270997), anhydrous pyridine (99.8% #270970), thionyl bromide (97% #251259), ammonia in tetrahydrofuran (0.4 M in THF #718939), ammonia in methanol (4M in methanol #779423), ammonia in isopropanol (2M in isopropanol #392693), anhydrous hydrazine (98% #215155), propargylamine (98% #P50900), N-Boc-propargylamine (97% #687146), *N*-hydroxysulfosuccinimide sodium salt (sulfo-NHS, 98% #56485) and 1-ethyl-3-(3-dimethylaminopropyl)carbodiimide hydrochloride (EDC, 98% #161462) were purchased from Sigma Aldrich (St. Louis, MO). Ammonia gas (99.99% anhydrous CAS#7664-41-7) was purchased from Praxair (Danbury, CT). Anhydrous dichloromethane (99.7%+ #41835) and anhydrous dimethyl sulfoxide (99.8% #43998) were purchased from Alfa Aesar (Haverhill, MA). 4-inch silicon wafers coated with a 10 nm titanium adhesion layer and 100 nm layer of gold were purchased from LGA Thin Films, Inc. (Santa Clara, CA).

Procedures.

Alcohol-rich HPHT Nanodiamond (ND-OH) preparation and storage

A three-zone tube furnace (Thermo Scientific STF55346COMC-1) was utilized to aerobically oxidize 30 nm and 50 nm HPHT nanodiamond (ND). Approximately 500 mg of NDs were aerobically oxidized in a ceramic boat at 525°C for 5 hours in open air conditions yielding a tannish powder and held at 150°C prior to removal from the tube furnace. Post oxidation yields were typically 60-65%. The NDs were then placed in a glass scintillation vial and inserted into a drying oven (~140°C) to ensure a water free ND surface prior to bromination chemistry. Water free ND-OH samples were stored in the drying oven until needed for further chemistry or spectroscopic characterization.

Glassware preparation, solvent preparation

All synthetic glassware, including 100 mL and 1000 mL single neck round bottom flasks, Pasteur pipettes, scintillation vials, stir bars and glass adapters were dried in a 140 °C drying oven to remove water 24 hours prior to the start of the bromination. Micropipettes or micropipette tips

containing any rubber or plastic pieces were dried at 40°C in a vacuum oven for 24 hours. Anhydrous solvents were poured over molecular sieves that were activated at 200°C in vacuo prior to the reactions into a 1000 mL round bottom flasks. The work was performed in a N₂ gas filled Inert Technologies HE-Purelab 4-port glovebox (Amesbury, MA).

ND-Br synthesis/purification

Reactions of ND-OH with thionyl bromide (SOBr₂) were setup inside of the N₂ glovebox and then transferred to a Schlenk line for 24 hours. Two different bromination reactions, with and without pyridine, were performed in 100 mL single neck round bottom flasks with a Teflon coated stir bar. The non-pyridine reactions were done by charging a round bottom flask with 120 mg of dry ND-OH, 2.5 mL SOBr₂ [1.27 M] and 10.0 mL DCM. The catalyzed reaction was done by charging a round bottom flask with 40 mg of ND-OH, 0.516 mL SOBr₂ [0.6M], 5.467 mL DCM and 0.591 mL of pyridine. Reaction flasks were sealed with a glass adapter, vacuum grease and metal keck clips and removed from the inert atmosphere glovebox and placed in a cup horn sonicator (Fisher Scientific FB505). Cup horn sonication was done at 75% power for five minutes (5 second on/off cycles) and immediately vortexed for one minute to fully disperse the mixture. The samples were then attached to a purged Schlenk line and stirred vigorously at 500 rpm with a N₂ flow rate of approximately 1 mL/second and allowed to react for 24 hours at 25°C. At the 6-hour mark, reactions would be removed from the Schlenk line, cup horn sonicated for 2 minutes and then returned to the Schlenk line for the remainder of the reaction. Three purge and fill cycles were used to remove oxygen and water from the connecting tubing of the Schlenk line to the reaction vessel. After 24 hours, the samples were removed from the Schlenk line, sonicated for five minutes using a bath sonicator (Branson 3800), vortexed and introduced into the glovebox. **NOTE: A bath sonicator was used to prevent high sample temperatures, yet energetic enough to break apart the pellet without removing bromine on the surface of the nanodiamonds. Use of a cup horn sonicator was found to spontaneously debrominate the surface and should be avoided.**

The pyridine sample contained a black pyridinium perbromide salt that was gelatinous, oily and was a reddish-black tone. The uncatalyzed reaction was bright orange in color. The catalyzed reaction required three purification cycles with DCM, one with DMSO, and a final wash with

DCM to conclude the sample workup. The DMSO solubilized the salt during the purification cycle and was complete after one addition. The uncatalyzed reaction only required three purification cycles with DCM. To purify the sample, the sample of ND-Br solution was transferred to a 50 mL polypropylene centrifuge (Beckman Coulter # 357003) tube and centrifuged at 21,000 RPM (50,000 rcf) for 30 minutes at 10°C. Note: Centrifugation at 25°C was found to debrominate the ND-Br and should be avoided. The ND-Br with pellet and supernatant was reintroduced into the glovebox, the supernatant was discarded as waste and the ND-Br pellet collected. To the ND-Br pellet was added 15-20 mL of anhydrous DCM or DMSO, bath sonicated and vortexed. The purification cycles were completed 3 times, during the final wash the supernatant would be optically clear and colorless. ND-Br samples were stored as solid powders or dispersed in 1 mg/mL in DCM for various experiments. Long term storage of ND-Br was in a 4°C refrigerator as a powder or in solution. ND-Br stability was limited to under 2 weeks and therefore the constructs should be used immediately for further chemistry.

ND-NH₂ preparation (includes both ammonia solution, condensed ammonia and gas phase)

In the glovebox, a 100 mL single neck round bottom flask was charged with 20 mgs of ND-Br, 1 mL of ammonia in THF [0.4M] and 9 mL of DCM. With propargylamine, a 100 mL roundbottom was charged with 20 mgs of ND-Br, 1.4 mL of propargylamine and 3.6 mL of DCM. In both reactions, the flasks were sealed with a glass adapter, attached onto a purged Schlenk line, and allowed to react for 24 hours while stirring vigorously. Bath sonication was used to disperse the ND-Br during the amination chemistry. Reactions can also be performed by sealing with a septum and allowed to react without a connection to the Schlenk line. Purification of ND-NH₂ was done with 10 mL DCM, for a total of three washes at 50,000 rcf for 30 minutes in polypropylene tubes, and a final wash with 10 mL of 18 MΩ water. Condensed NH₃ chemistry was performed by placing 20 mg of ND-Br in a 100 mL round bottom in the glovebox and placing it on the Schlenk line and placing it under vacuum. The round bottom was submerged in an isopropanol and dry ice bath and then back filled with anhydrous ammonia gas and allowed to react as a liquid over neat NH₃ for 30 minutes. The sample was then allowed to warm to 25°C and the NH₃ returned to the gas phase and yielded a dry aminated ND powder. The ND-NH₂ powder was then purified 3 times with 18 MΩ water and stored at 1 mg/mL solution in water.

Gaseous amination was carried out in a three-zone tube furnace using NH_3 gas at elevated temperatures. In a typical reaction 20-40 mg of ND-Br was loaded into ceramic boats, the boats were inserted into a 50 mL centrifuge tube inside the glovebox, sealed and inserted into the tube furnace under inert conditions. A plastic purging bag with arm slots were connected to the mouth of the tube furnace and purged for 1 hour prior to opening the sealed samples tubes. After 1 hour the tubes were opened the ceramic boats were removed and the samples placed into the quartz tube furnace chamber. The positions of the boats were adjusted to cover the range of 200–700 °C. After introduction 3 purge and fill cycles were performed on the tube furnace environment prior to NH_3 introduction and elevation of the temperature. The furnace was then filled with ammonia gas (50 sccm flow rate) with a N_2 carrier gas (100 sccm flow rate) and reacted for 2 hours. After the reaction, ammonia was purged for 30 minutes with nitrogen at 1000 sccm and the samples removed. The ND- NH_2 samples were stored in ambient conditions and dispersed in water at 1 mg/mL concentrations.

Open air and inert atmosphere DRIFTS and TPD-DRIFTS

DRIFTS measurements were performed using the Harrick Praying Mantis DRIFTS attachment (DRK-3), high temperature reaction chamber (Harrick #HVC-DRM-5) and a Thermo Fisher FTIR (6700) equipped with MCT/A detector. The high temperature reaction chamber was cleaned and stored in the vacuum oven prior to being brought back into the glovebox. OMNIC software controlled the Thermo 6700 instrument. Temperature control of the DRIFTS chamber was controlled by Harrick software. DRIFTS measurements were performed with 128 scans at a resolution of 2 cm^{-1} and background scans of near or equal signal intensity. KBr powder was stored in an oven (120 °C) 24 hours prior being brought into the glovebox. When bringing the KBr or DRIFTS chamber into the glovebox, three 3-minute purge and fill cycles were performed to remove any oxygen and water. All DRIFTS work was performed inside the glovebox under inert conditions. For collecting background data, 80 mgs of the dried KBr was used and filled the DRIFTS cup completely. Using a mortar and pestle, the KBr was ground into a fine powder, introduced into the cup and the excess KBr was then leveled with a sample preparation tool leaving a flat and gouge-free KBr surface. The IR reflectance spectrum scans were set at 128 scans and the background data were collected. The saved background data was then applied for subsequent

data collection. This process was repeated for temperature dependent studies and the background files were saved. For collecting sample data 3-4 mgs of ND-OH, ND-Br or ND-NH₂ were added to 80-90 mg of KBr and mixed thoroughly. Sample DRIFTS data was collected in percent reflectance mode with a representative background scan.

DRIFTS parameters and Analysis. Kubelka-Munk transformations were performed individually with linear background corrections in Igor Pro software. Linear backgrounds were generated based on the averaged values of percent reflectance (raw data) in the DRIFTS regions of 2000 - 2200 cm⁻¹ and 3800 - 4000 cm⁻¹. This slope value was then applied to a y-intercept function ($y=mx+b$) and applied to spectra for normalized reflectance units (R) and then transformed using the Kubelka-Munk equation to make the data proportional to concentration:

$$KM\ Units = \frac{(1-R^2)}{2R} \quad (1)$$

Infrared values were cross referenced to *Infrared and Raman characteristic group frequencies: tables and charts* by Socrates and HPHT ND studies.⁷⁻¹¹

ND-OH, ND-Br and ND-NH₂ deposition on Gold Coated Silicon Wafers for XAS, XPS and XES experimentation.

Gold-coated silicon wafers from LGA thin films (Santa Clara, CA) were cut into 1 x 1 cm squares, bath sonicated in acetone, isopropanol, 18 MΩ water three times, and dried with a N₂ gun. The wafers were then etched for a minimum of 10 minutes with a piranha solution (90 mL concentrated sulfuric acid and 10 mL hydrogen peroxide), with the gold layer facing upwards in a crystallizing dish. After drying the etched Au wafer, 300 μl of 1 mg/mL ND solution was deposited and dried onto the substrate and covered with a crystallizing dish. Moisture-sensitive brominated nanodiamond samples were prepared in an inert atmosphere glove box using dichloromethane as the solvent in a similar fashion. Piranha etched wafers were dried for 24 hours at 140°C prior to be introduced into the glovebox and ND-Br being deposited to insure a water free surface. Oxidized and aminated nanodiamond samples were prepared using 18 MΩ water as a solvent under open-air conditions at 1 mg/mL concentrations. Note: A 10 nm Ti or Cr adhesion layer is used

prior to 100 nm gold deposition on Si substrates. Piranha etching did cause pin hole etching of the gold and adhesion layers and Si XPS signals were observed.

Synchrotron XAS data collection, PFY-XAS/XES analysis and RIXS Measurements

X-ray absorption (XAS) and resonant inelastic X-ray scattering (RIXS) measurements were performed at beamline 8-2 and 10-1 at the Stanford Synchrotron Radiation Lightsource, SLAC National Accelerator Laboratory using a spot size of $< 1 \text{ mm}^2$. All samples were handled in an inert atmosphere glovebox and mounted to an Al sample bar with conductive carbon tape (#16073-4 Ted Pella, Inc. Redding, CA). The samples were transported to the beamline in a sealed polypropylene jar and a magnetic mounting piece was attached to the sample bar in inert atmosphere glovebox. The sample bar was then brought to the beamline and purged with N_2 gas for 60 minutes inside a plastic glove hands attached to the transfer chamber. Once purged, the transfer chamber was vented and the sample bar was introduced into the transfer chamber under a positive pressure N_2 flow. Samples were introduced into the analysis chamber after the transfer chamber reached 1×10^{-7} torr. Analysis chamber conditions were typically conducted at 5×10^{-9} torr.

At 8-2 and 10-1, carbon, nitrogen and oxygen K-edge XAS was measured in total electron yield (TEY) mode using $42 \times 42 \text{ }\mu\text{m}$, $40 \times 40 \text{ }\mu\text{m}$, and $30 \times 30 \text{ }\mu\text{m}$ slits, respectively. TEY mode probes approximately 5-10 nm of the sample depth and all experiments were conducted under ultrahigh vacuum conditions ($\sim 5 \times 10^{-9}$ torr). After focusing the optics, the reference absorption intensity of the incoming X-ray beam was measured using a sample of gold coated mesh and used to correct for beam instability. XAS data was collected at an incident electric field vector of 54.7° . For spectral analysis the data was treated with a linear pre-edge background subtraction from a region before the absorption edge of carbon, nitrogen and oxygen at 260 - 280 eV, 370-380 eV and 510 - 530 eV, respectively. A post-edge normalization was also performed in the continuum region at 340 eV for carbon, 420 eV for nitrogen and 580 eV for oxygen and performed using a batch processing macro in Igor Pro. Energy calibration was performed using the signal from the diamond core-hole exciton which is determined to be 289.0 eV as described elsewhere.¹² X-ray energy calibration of the synchrotron light source was performed during grating changes with a Ni slab (Ni L3 absorption) and a 1-point fitting procedure.

RIXS measurements were performed using the super conducting transition edge sensor (TES) X-ray detector as described elsewhere by Lee and Titus.¹³⁻¹⁴ The TES allows for background-free X-ray detection without a diffraction grating and good energy resolution (1 eV). A resonant inelastic X-ray scattering (RIXS) measurement is performed by sweeping across the excitation monochromator photon energies and collecting a time-tagged X-ray pattern across the TES detector. The TES allows for all photons to be simultaneously collected across all detector elements in the array. Analysis of the RIXS data produced by the TES detector is covered thoroughly by Lee et al.

Laboratory XPS Measurements and Analysis

A Thermo Scientific K-Alpha Surface Analysis XPS instrument at the Molecular Foundry was utilized to probe for carbon, nitrogen, and bromine signals on the surface of the ND-Br and ND-NH₂ samples. The K-Alpha Plus XPS has a combined low energy electron and ion flood source and are utilized to suppress charging during all data collection. The XPS X-ray source and detector is an Al K α micro-focused monochromator and is equipped with a 180° double hemispherical analyzer with a 128-channel detector. The low resolution and high-resolution pass energy are 200.0 eV and 50.0 eV, respectively. The low resolution and high-resolution energy step size are 1.0 eV and 0.1 eV, respectively. For high-resolution scans, 50 scans were taken of bromine and nitrogen and 10 scans for oxygen and carbon to ensure good signal to noise and a dwell time of 50 ms. The electron acceptance angle was 55° and survey scans were performed over a binding energy range from 0-1350 eV, a pass energy of 200 eV, 3 scans were summed and a dwell time of 10 ms was used. ND-Br samples that required air-free transfer from the glove box to the K-alpha XPS instrument were loaded into the inert atmosphere transfer module. ND-Br samples were loaded into the transfer module for analysis and transported from SJSU to The Molecular Foundry.

XPS analysis was performed using Igor Pro software and the CASA-XPS software package and standard background subtraction and fitting protocols were followed on survey and high-resolution scans. For example, a linear background subtraction was performed on N1s high resolution scans in Igor Pro and then peaks were fit to a Voigt line shape with a mixed Gaussian and Lorentzian contribution. Peak widths were typically held to a FWHM of 1.5-2.0 eV as

appropriate for the spectral features. Quantitative analysis of survey scans to determine the atomic percentage of individual elements was performed using CASAXPS software and Tougaard backgrounds were applied with relative sensitive factors (RSF) values being applied for each element. RSF values for C, N, O and Br were 1.0, 1.8, 2.93 and 2.8, respectively. Percentage atomic concentrations () are calculated using equation:

$$X_A = \frac{(I_A E^\alpha)/(R_A T(E))}{\sum (I_i E^\alpha)/(R_i T(E))} \quad (2)$$

Wherein, X is the atomic percentage of element A, R_i is the RSF for the relative intensity I_i and T(E) is the transmission function of the instrument for intensity I_i at kinetic energy (E).⁶ The alpha term in the exponent of kinetic energy E is used to adjust for analyzer specifications. The VAMAS (Versailles Project on Advanced Materials and Standards) file collected by the K-Alpha instrument allowed for all needed transmission function information to be applied for quantification purposes and the VAMAS file type is ISO 14976 compliant. XPS features from the thin film substrate include Au4f, Si2p and Ti3s found at 85 eV, 99 eV and 59 eV, respectively.

Table S1: Inelastic mean free paths of C1s, N1s, O1s and Br3d electrons based on Seah¹⁻² and sensitivity factors based on transmission functions in VAMAS files.^{4,6}

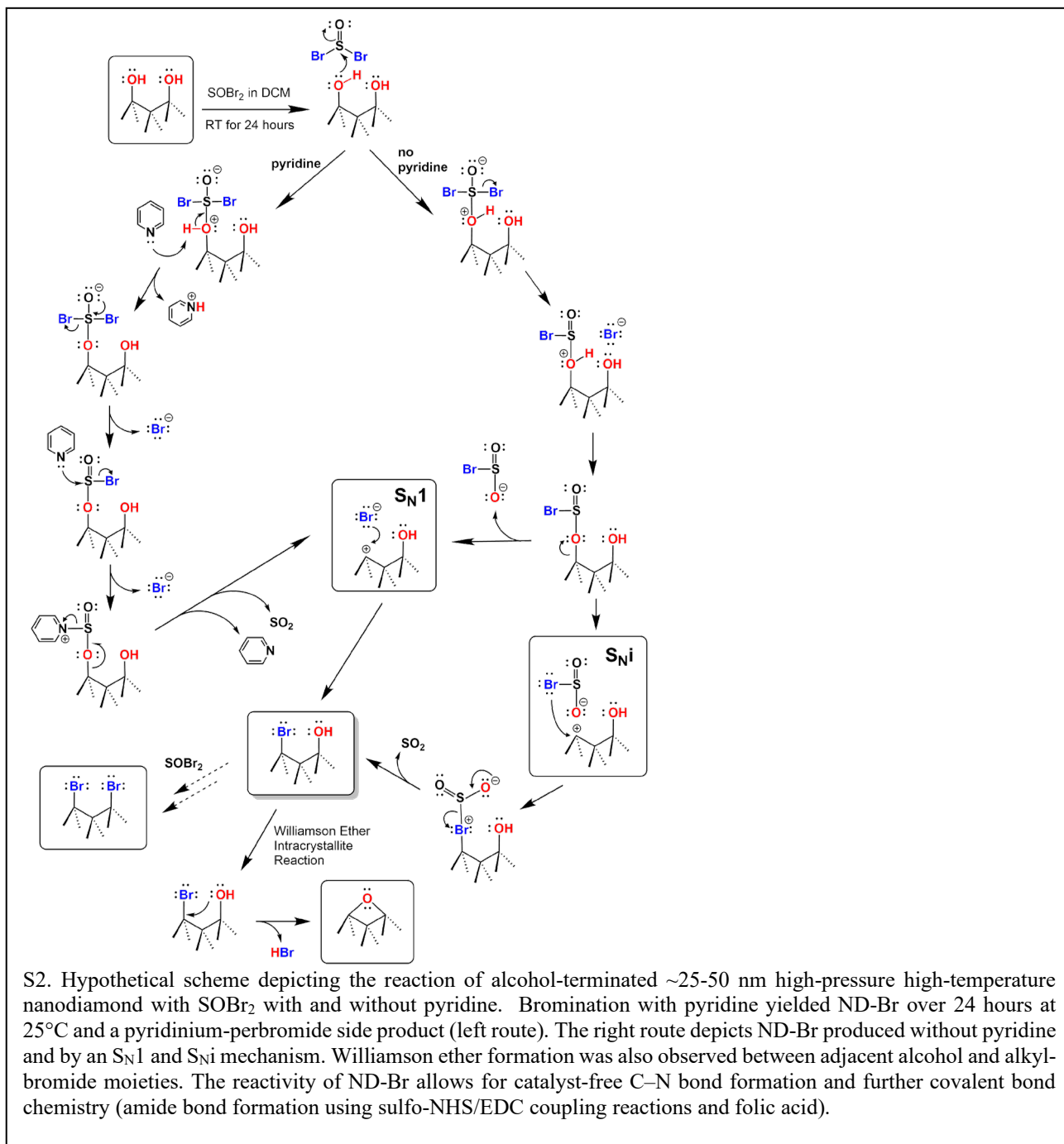
Element	Edge	IMPF (nm)	Sensitivity factors
Carbon	1s	1.87	1.0
Nitrogen	1s	1.78	1.8
Oxygen	1s	1.67	2.93
Bromine	3d	2.03	2.8

Results and Discussion Sections #1-7

1. Time dependent study of bromination chemistry with and without pyridine

Addition of pyridine accelerated the SOBr_2 bromination of ND-OH constructs and also produced a viscous side product of pyridinium tribromide (PTB) ($\text{NC}_5\text{H}_5 \cdot \text{HBr} \cdot \text{Br}_2$).¹⁵⁻¹⁶ The PTB side product was removed with a single DMSO washing step and the salt could be observed in a portion of the decanted supernatant (Figure S1). Lack of pyridine during bromination resulted in alkyl-bromide formation as seen in S3 and did not require a DMSO purification step. Post purification samples produced a light tan to light greyish tone for the pelleted samples and the

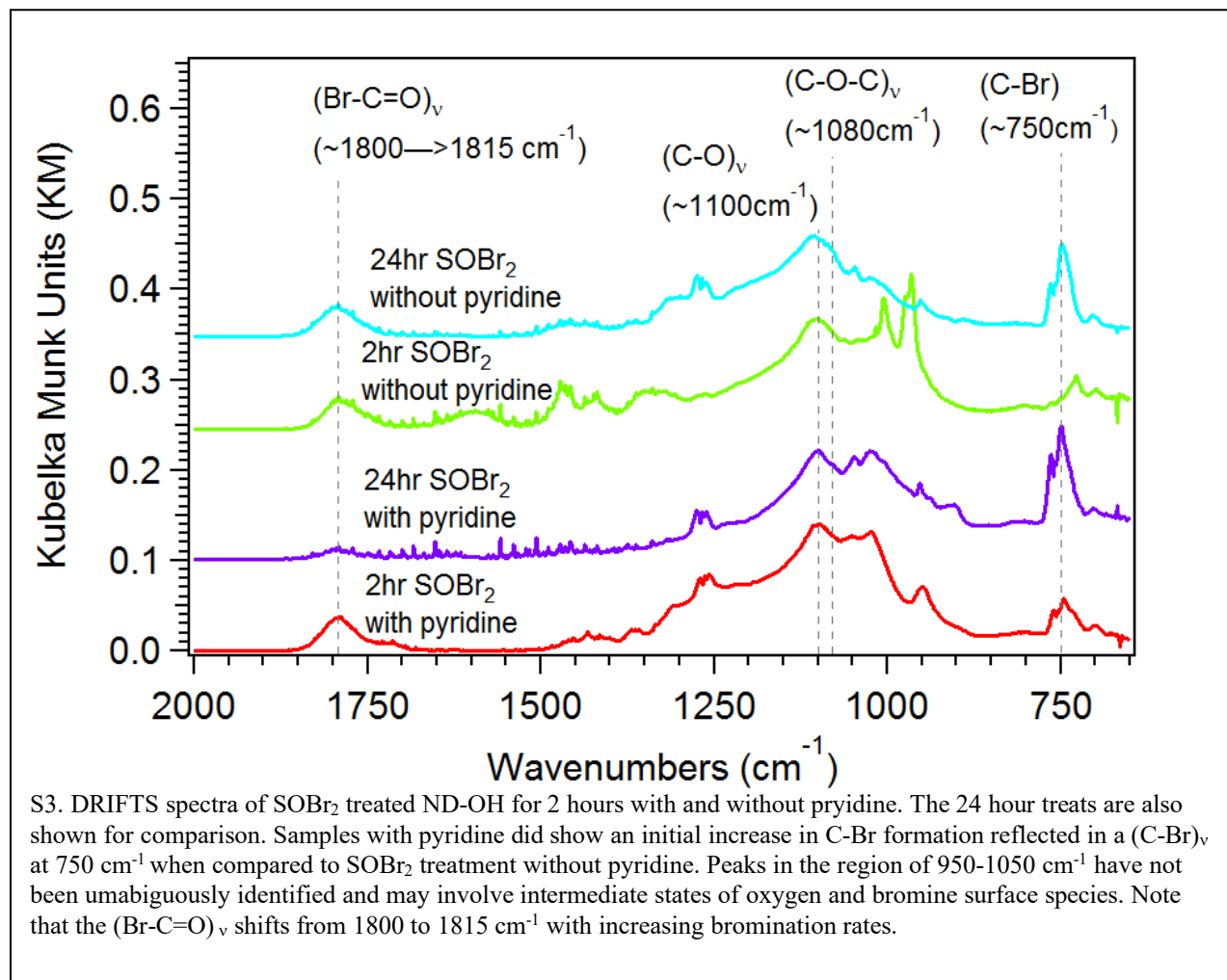




supernatant would be optically clear and colorless after 3 purification cycles. A mechanistic scheme for bromination is depicted in S2.

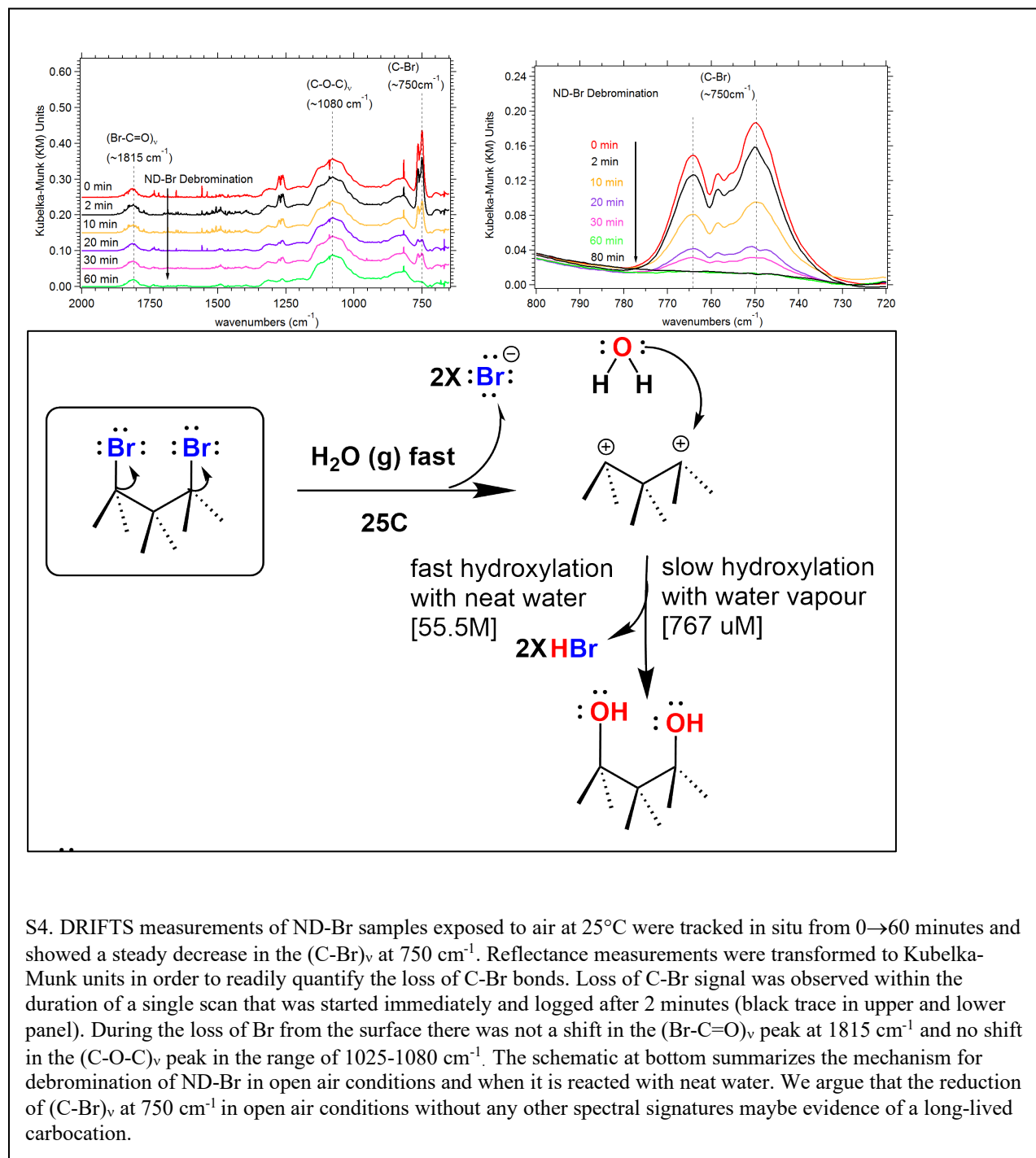
The increased rate of ND-Br formation with pyridine can be observed when comparing the 2 hour and 24 hour DRIFTS data. The increased ND-Br reaction is tracked through the emergence of the $(\text{C-Br})_v$ stretching mode at 750 cm^{-1} (Figure S3). The $(\text{C=O})_v$ of carboxylic acids at 1780 cm^{-1} shifts to 1815 cm^{-1} during the bromination process and is assigned to an acid bromide. Peaks arise in the $950\text{-}1050\text{ cm}^{-1}$ region as early as 2 hours and are not static between any of the reaction

conditions. Assignment of the 950-1050 cm^{-1} region has not been completed and is most likely due to oxygen and bromine containing intermediates on the diamond surface. The peak at 1025 cm^{-1} is assigned to the $(\text{C-O-C})_v$ bridging vibrational mode of an ether moiety caused by the intracrystallite Williamson ether-like surface reaction.¹⁷⁻¹⁸ The sample surface is free of physisorbed water as evidenced by the lack of a $(\text{O-H})_s$ mode at 1630 cm^{-1} .

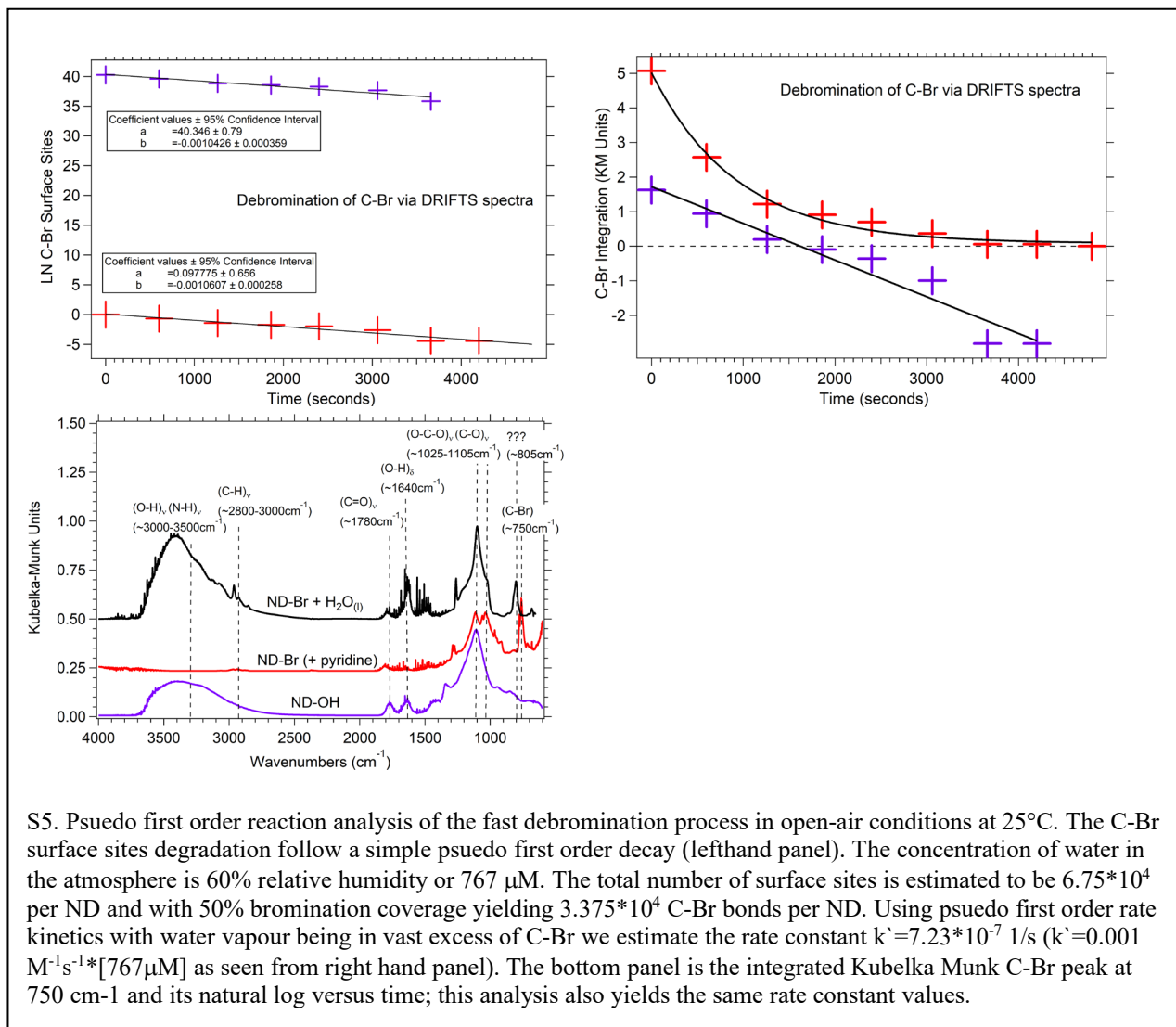


2. Debromination and analysis of ND-Br in open air conditions.

The instability of the C-Br bond on the HPHT nanodiamond surface is clearly illustrated by DRIFTS measurements at 25°C. A ND-Br sample was observed to have a strong (C-Br)_v peak at 750 cm⁻¹ in inert conditions using the Harrick inert atmosphere chamber. To initiate the debromination, two VCO caps were removed from the Harrick chamber and the DRIFTS



spectra was collected at various time points until the C-Br vibrational mode was extinguished. As early as the first scan collected within 5 seconds of the VCO cap opening there was a detectable decrease in (C-Br)_v peak intensity and is labeled a 2-minute scan (Figure S4). Data collection of 128 scans at 2 cm⁻¹ resolution takes approximately 2 minutes. This instantaneous degradation of the C-Br bond is highly unusual and is not consistent with other bromide derivatives such as 1-bromoadamantane, which can be handled in open air conditions without degradation. In contrast, hydrolysis studies of 1-bromoadamantane with NaOH in a water-toluene-polymer tri-phasic system required 0.1 M NaOH at 100°C in the presence of a catalyst to generate 1-hydroxyadamantane.¹⁹



S5. Pseudo first order reaction analysis of the fast debromination process in open-air conditions at 25°C. The C-Br surface sites degradation follow a simple pseudo first order decay (lefthand panel). The concentration of water in the atmosphere is 60% relative humidity or 767 μM. The total number of surface sites is estimated to be 6.75*10⁴ per ND and with 50% bromination coverage yielding 3.375*10⁴ C-Br bonds per ND. Using pseudo first order rate kinetics with water vapour being in vast excess of C-Br we estimate the rate constant k' = 7.23*10⁻⁷ 1/s (k' = 0.001 M⁻¹s⁻¹*[767μM]) as seen from right hand panel). The bottom panel is the integrated Kubelka Munk C-Br peak at 750 cm⁻¹ and its natural log versus time; this analysis also yields the same rate constant values.

Kinetic analysis of the debromination process shown in S5 reveals that the loss of C-Br bonds at 25°C in open air conditions was best modeled as a pseudo first order reaction in a reaction scheme similar to:



$$Rate = k_1[ND - Br][H_2O] \quad (5)$$

$$Rate = k_1^{\prime}[ND - Br] \quad (6)$$

$$k_1^{\prime} = k_1[H_2O] \quad (7)$$

The observations based on DRIFTS suggest that a long lived “radical carbon” or other reactive intermediate on the ND surface may exist for 80 minutes or longer at 25°C.²⁰⁻²¹ Prediction of a “radical carbon” based on brominated diamond was found through DFT by Larsson and Lunell and was not observed with chlorine or fluorine termination.²² An analogous system would be that of 8,9-dehydro-2-adamantyl with a stable carbocation at -120°C and confirmed via ¹H and ¹³C NMR.²¹ NMR is not sensitive enough to be used for surface analysis of HPHT ND samples and therefore such experiments are not appropriate. In-situ gas phase amination will be required to reinforce the time dependent formation of amines on the diamond surface. The lability of the C-Br bond, the unique properties of diamond and the low concentration of water molecules in atmospheric conditions have aided this observation. Exposure to water in the gas or liquid phase leads to the loss of carbon-bromine bonds and anhydrous conditions should be followed.

No observed rehydroxylation of the sample occurred during the 80-minute experiment because we do not observe an increase or return of the (C-O)_v mode at 1105 cm⁻¹ representative of alcohol-

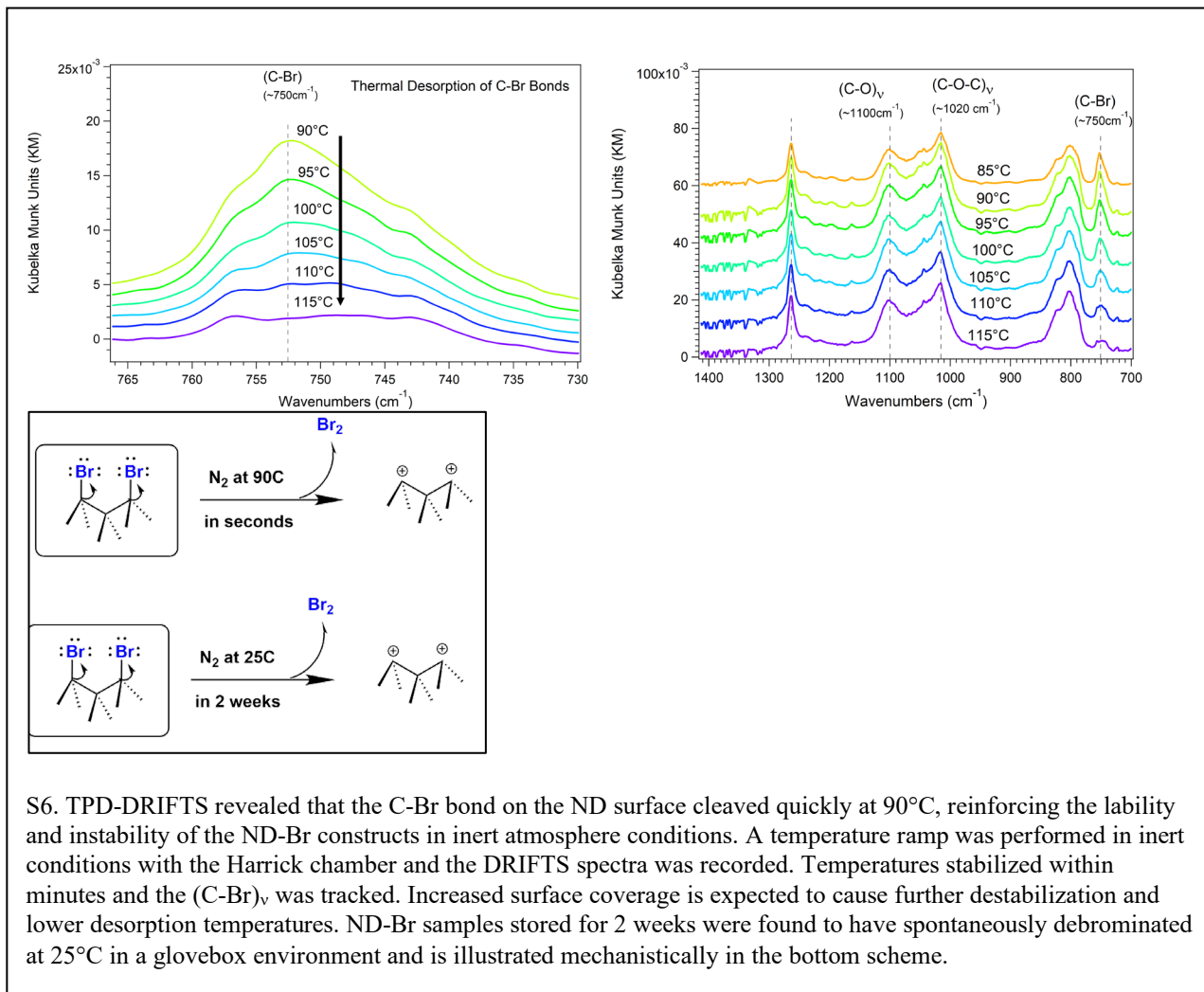
rich NDs, and no shifting or movement of line shapes occur during the air-exposure. Our conclusion is that rehydroxylation is slow compared to the debromination kinetics with 60% relative humidity at 25°C [767 μM]. Pseudo 1st order reaction analysis yields a rate constant $k' = 7.23 \times 10^{-7} \text{ 1/s}$ ($k' = 0.001 \text{ M}^{-1}\text{s}^{-1} \times [767 \mu\text{M}]$) as seen from panels in Figure S5. As a control, ND-Br was reacted with 2 mL of 18 M Ω water [55.5 M], purified by centrifugation and probed with DRIFTS and shows the reemergence of an alcohol-rich surface within 1 minute of reaction time (Figure S5 bottom left panel). Based on the molarity of pure water, the pseudo 1st order rate of $k' = 0.055 \text{ 1/s}$ ($k' = 0.001 \text{ M}^{-1}\text{s}^{-1} \times [55.5 \text{M}]$), an increase of 7.2×10^4 in the pseudo first order experimental rate. Based on a reaction in water, the rehydroxylation reaction in neat water would be complete in 66 ms.

3. Debromination and analysis of ND-Br during thermal desorption under Inert Conditions.

Instantaneous covalent bond dissociation of the carbon-bromine bond on the nanodiamond surface was observed at 90°C, consistent with a highly labile leaving group on the diamond surface. Temperature programmed desorption-DRIFTS or TPD-DRIFTS allows the stability of the C-Br bond to be examined in inert conditions. Samples are loaded into the Harrick high temperature reaction chamber in the inert atmosphere glovebox and the TPD-DRIFTS measurements occurred from 70-120°C. To insure proper TPD-DRIFTS, KBr backgrounds at experimental temperatures were taken and applied for each spectrum collected. Data for 85-115°C are displayed in S6. Noticeable reduction in the (C-Br)_v peak was observed at 90°C within 2 minutes of the temperature being reached.

Importantly, we found that over a 2 week period, the ND-Br samples would debrominate in the glovebox at 25°C (data not shown) and highlights that the C-Br bond dissociation mechanism is active at 25°C, but is slow compared to our experimental temperature of 90°C. Our findings are consistent with a weakening of the carbon-halide bond on the diamond surface as the halide identity changes from fluorine, chlorine and bromine atoms.²³ Previous studies showed that thermal bond dissociation of carbon-fluoride and carbon-chloride bonds on single crystal diamond

were observed to occur from 227-920 °C and 150°C, respectively.²⁴ A further temperature reduction below 150°C is reasonable and observing spontaneous C-Br dissociation at 90°C within the TPD-DRIFTS measurement time of 2 minutes indicates the reaction is kinetically fast. Bond



S6. TPD-DRIFTS revealed that the C-Br bond on the ND surface cleaved quickly at 90°C, reinforcing the lability and instability of the ND-Br constructs in inert atmosphere conditions. A temperature ramp was performed in inert conditions with the Harrick chamber and the DRIFTS spectra was recorded. Temperatures stabilized within minutes and the (C-Br)_v was tracked. Increased surface coverage is expected to cause further destabilization and lower desorption temperatures. ND-Br samples stored for 2 weeks were found to have spontaneously debrominated at 25°C in a glovebox environment and is illustrated mechanistically in the bottom scheme.

dissociation energies have not been derived in this study but are expected to be less than 2.21 eV/bond or 214 kJ/mol as calculated for 1-bromoaniline using G4 thermochemical calculation.²⁵

4. Nanodiamond surface analysis based on XPS Survey Scans.

4A. Equations governing C1s XPS signal and attenuation due to surface species. Quantitative elemental analysis of the ND surface was performed with the survey scans of the respective samples. The quantification required 2 steps; 1) quantitative analysis based on the CASAXPS software package assuming a uniform distribution of the elements with resulting atomic percentage concentrations and 2) applying a simple model that represents the surface coverage of heteroatoms nitrogen, oxygen and bromine on the nanodiamond substrate and the attenuation of the C1s signals. Recall that relative sensitive factors (RSF) values being applied for each element are seen in equation 2. RSF values for C, N, O and Br are 1.0, 1.8, 2.93 and 2.8, respectively, and shown in table S1. RSF values used in the CASAXPS analysis package are a function of Scofield cross sections at the Al K α X-ray emission wavelength and are used to calculate the percentage atomic concentrations.

The inelastic mean free paths (IMFP) of C1s, N1s, O1s and Br3d photoemitted electrons from the sample are calculated to be ~1.7-2.0 nm with the Al K α (h ν =1486.6 eV) source used in this study. These IMFP values are calculated from Seah and Dench based on binding energies of 284 eV, 399 eV, 532 eV and 70 eV for C1s, N1s, O1s and Br3d, respectively and the universal IMFP equation,

$$\lambda = \frac{143}{E^2} + 0.054 * \sqrt{E} \quad (8)$$

wherein, λ and E are the inelastic mean free path and energy of the electron in electron volts (eV).¹ Additional versions of the IMFP equation have been presented by Seah, but will not be covered here.²⁶⁻²⁷ Because N1s, O1s and Br3d species will only be present as an atomic layer at the diamond surface, the IMFP is not relevant for those elements ($\lambda_{C1s}=\lambda_{N1s}$). Therefore, the C1s photoemitted electrons are the only XPS signal limited by the IMFP and table S2 summarizes our results of several samples for alcohol, bromine and amine terminated NDs.

The C1s XPS intensity and attenuation is based on a IMFP of 1.87 nm and is given by

$$I(d) = I_0 e^{-d/\lambda} \quad (9)$$

wherein I(d) is the signal intensity as a function of d in nm, I₀ is the initial intensity in a pure substance and λ is the IMFP. Solving for distance (d) based on the observed intensity yields,

$$-d = \ln\left(\frac{I(d)}{I_0}\right) * \lambda \quad (10)$$

In a similar expression given by Kono et al. they express the C1s XPS intensity by,

$$I_{1C1s} = C * C_c * \sigma_{C1s} * T_{C1s} * \int_0^\infty e^{-\frac{z}{\lambda_{C1s} * \cos \theta}} dz \quad (11)$$

where C is an instrument constant based on photon flux and geometry, C_c is the concentration of carbon atoms in diamond, σ_{C1s} is the photoionization cross section, T_{C1s} is the transmission function for the electron analyzer, λ_{C1s} is the mean free path and z is the depth from the top of the diamond surface. $\sigma_{C1s} * T_{C1s}$ is commonly known as the relative sensitivity factor (RSF) and given as 1.0 for carbon and can be seen in table S1. All elements in the CASAXPS software use a specific RSF based on the instrument configuration, photoionization cross sections and transmission function. Measurement of a thin homogenous layer that dampens the C1s signal is then described by

$$d = \lambda_{imp} * \cos \theta * \left(\frac{I_{imp}}{I_{C1s}}\right) * \left(\frac{\sigma_{C1s}}{\sigma_{imp}}\right) * \left(\frac{T_{C1s}}{T_{imp}}\right) * \left(\frac{\lambda_{C1s}}{\lambda_{imp}}\right) \quad (12)$$

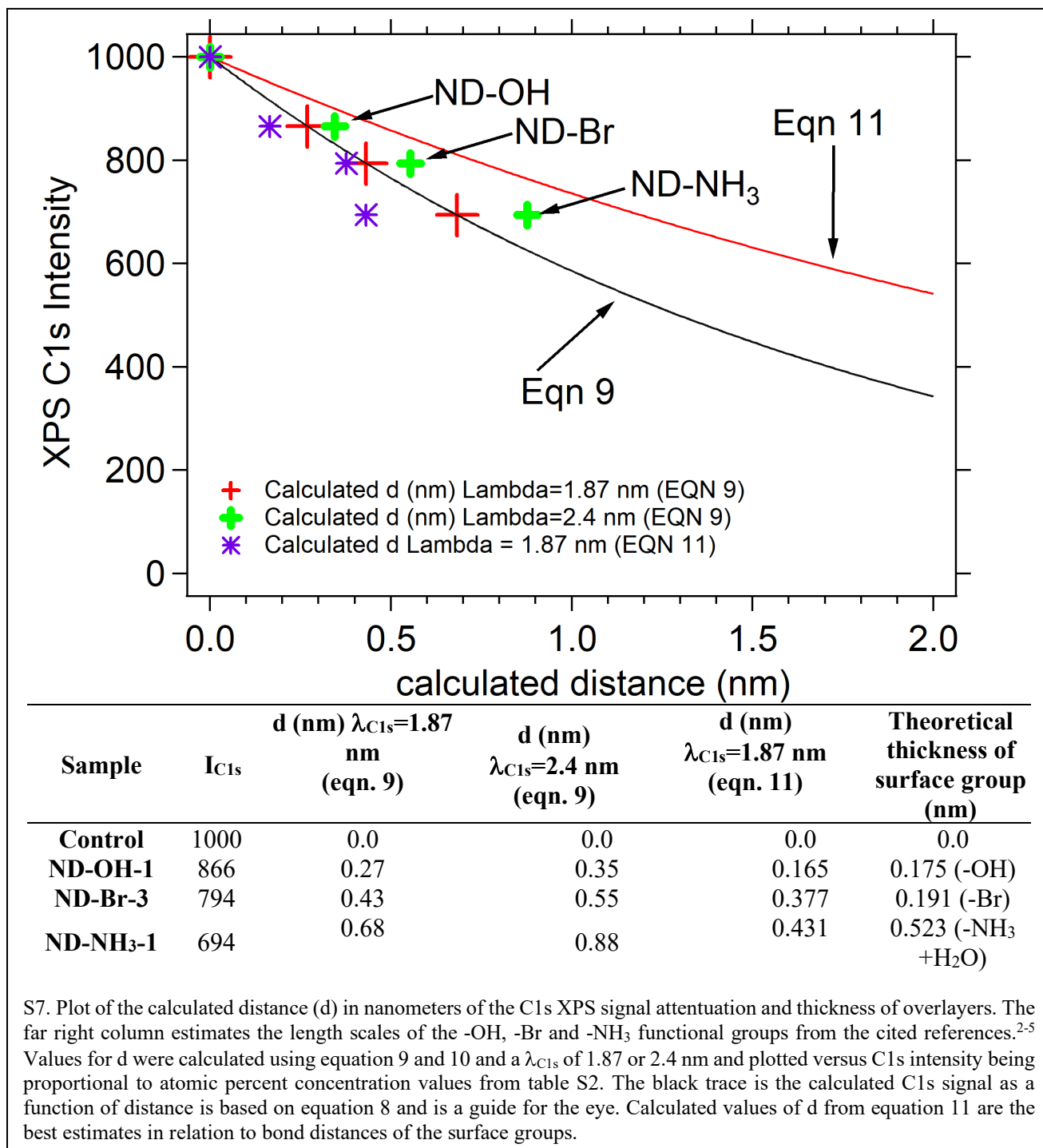
wherein the λ_{imp} is assumed to be the same as λ_{C1s} and $\theta=55^\circ$ across all measurements.

Because all other XPS signals are from a monolayer (ML) or less, their respective IMPFs for N1s, O1s and Br3d are not needed as they are not attenuated as a function of distance. Kono et al. states that the overlayer has the same IMFP as C1s electrons as seen in equation 11 and $\lambda_{C1s}=\lambda_{N1s}$ ($\lambda_{C1s}=\lambda_{O1s}$, $\lambda_{C1s}=\lambda_{Br3d}$), is assumed in this study as well.

4B. Analysis of C1s signal attenuation as a function of distance and overlayer thickness (d).

Using equation 9, the natural log of attenuated experimental intensity over the initial intensity (value =1000) and λ_{C1s} was used to calculate d in nanometers as seen in the red crosses of S7 and plotted. The signal decay scales as $e^{-(d/\lambda)}$ and a theoretical C1s plot based on equation 9 with the attenuated intensity as a function of d is used as a guide for the eye. The value of d in nanometers is the estimated overlayer thickness of oxygen species (hydroxyls), bromines (alkyl-bromides) and nitrogen (amines) species and is given as 0.27 nm, 0.43 nm and 0.68 nm, respectively as seen in S7. The bond distances of hydroxyl, alkyl bromides and amine moieties on diamond surfaces have been calculated via DFT previously. Loh et al. calculated the C-O bond distance of hydroxyls on

111 to be 0.141 nm, O-H bonds to be 0.0995 nm and a C-O-H bond angle of 109.7°.³ Tiwari calculated a C-Br bond distance of 0.191 nm at 50% bromine coverage and a C-C-Br bond angle of 107.3°.⁴ Miyamoto and Saito model the diamond surface with surface nitrogen and find the C-N bond distance to be elongated to 0.189 nm (second layer) and 0.232 nm (top layer) when hydrogen atoms are present and bound to nitrogen.² Miller found amine terminated diamond to



have N-H bond distances of 0.0985 nm when hydrogen bonding is considering and a H-N-H bond angle of 106.3°, but did not state C-N bond distances or C-N-H bond angles.⁵ The elongation of the C-N bond distance at the diamond surface is consistent with the observed decrease in C1s signal in ND-NH₃ samples and calculated overlayer distance (d) of 0.68 nm as found in S7 and table S2 values. Water adsorption of 1 ML is the cause of the increase in O1s % signals after amination chemistry, and is also supported by increased water adsorption in DRIFTS measurements seen in Figure 1B in the main article. ND-NH₃ samples were deposited from an aqueous solution onto the Au coated wafers and allowed to dry gradually. de Theije used DFT to model adsorbed water on hydroxyl terminated diamond and found a relaxed structure of 0.250 nm between adsorbed water and surface hydroxyl groups.²⁸ In total, based on DFT calculations, a 0.523 nm overlayer thickness in the ND-NH₃ samples is predicted which is close to the calculated d value of 0.431 nm using equation 11 based on our experimental XPS data (see S7). Equations 9 (black trace) and 11 (red trace) in figure S7 overestimate the thickness of the overlayer based on C1s intensity for all samples investigated when compared to theoretical bond distances as summarized above and in the far-right column of the S7 table. Equation 11 from Kono provides the best thickness values based on experimental XPS data in comparison to DFT. Equation 11 both underestimates (ND-OH and ND-NH₃) and overestimates (ND-Br) the overlayer thickness values with deviations of - 0.010 nm, +0.186 nm and -0.092 nm for ND-OH, ND-Br and ND-NH₃, respectively.

4C. Model for quantifying surface functional groups on HPHT NDs. Our model for determining the percentage of surface sites that were functionalized with alcohols, bromides or amines is based on assuming that all carbon signals originate from the diamond nanoparticle, atomic percent concentrations are taken from XPS survey scans, that C1s signals are attenuated as a function of overlayer thickness and that alcohol rich ND surfaces provides a upper limit of 15% O1s atomic percent concentration when no adsorbed water is present. Because the ND-OH samples were dried prior to XPS measurements and mounted in the glovebox, we estimate that no adsorbed water is present for the control sample. The initial model for HPHT ND-OH surfaces assumes near complete coverage of alcohols on the surface and would be equivalent to a 15% atomic percent concentration as described by Wang et al on single crystal diamond.²⁹ Wang et al. describes a 12%

and 16% oxygen content on the 111 and 100 diamond facets through XPS characterization, respectively. No ND-OH control sample data exceeded 14.2% of oxygen species based on survey scan analysis (see table S2 and S8). The 15% upper limit of oxygen surface species on HPHT ND-OH is reasonable considering increased surface roughness and increased surface to volume ratio of the 30-50 nm NDs. Additionally, 1 monolayer (ML) of alcohols is equivalent to approximately 18.2 alcohols per nm² on the 111 surface and is used throughout our calculations in Table S3.³⁰

4D. Conversion of survey scan quantification results in Table S2 to ND surface % in Table S3.

Elemental quantification from XPS survey scans is provided in Table S2, data provided in figure S8 and is based on the relative sensitivity factors and backgrounds previously described. To convert between the distributed atomic percentages provided by CASAXPS and yield a meaningful surface termination we use the following procedure. Atomic % for oxygen of ND-OH is 15% at a full alcohol termination and the calculated oxygen % in table S2 is divided by the maximum of 15% and the ratio estimates the alcohol termination present at the diamond surface. For example, ND-OH-1 in table S2 has a 13.4% oxygen content and therefore represents an alcohol coverage of 89.3% and is then multiplied by 18.2 surface groups/nm² on the 111 facet to provide the value of 16.3 alcohols/nm² in parentheses. ND-OH-2 with a 14.2 % oxygen content is then calculated to have a 95% alcohol coverage with 17.3 alcohols/nm². ND-Br sample calculations follow the same method, but are complicated by spontaneous C-Br bond cleavage in ultrahigh vacuum conditions that decreases the initial bromine concentrations. Based on this method, ND-Br-1 with 0.5% Br content is determined to have a 3.3% Br coverage or 0.6 alkyl-bromides/nm². The alcohol coverage is the remaining surface coverage of 96.7% or 17.6 alcohols/nm² in table S3. The actual Br coverage prior to debromination is higher and explained in conjunction with the amine results at the end of the section. Notice that the oxygen % for ND-Br-1 is 20.1% in table S2 and is over the established 15% of ND-OH control samples and is caused by the attenuation of the C1s signal by the larger thickness (d) of the brominated surface C-Br bonds. The oxygen surface content (caused by either alcohol or ether moieties via Williamson ether rearrangement) is therefore an overestimate and an accurate value is not known.

ND-NH₃ sample calculations are more accurate because the sole source of nitrogen atoms comes from C-N bond formation at the diamond surface and photoemitted N1s electrons are not attenuated. In an example calculation, ND-NH₃-1 has a 7.8% nitrogen content from table S2 and represents an amine surface coverage of 52% or 9.5 amines/nm² and a balance of 48% alcohols or 8.7 alcohols/nm². This value is calculated by dividing the nitrogen % by the maximum oxygen % of 15% from the dry ND-OH samples. The exchange of N atoms for O atoms must be a 1:1 ratio due to the alcohol to amine surface transformation during the S_N1 or E1 mechanism following the debromination process. Additional % oxygen content is from ~1 ML of physically adsorbed water that increases the oxygen % to 22.8%. The attenuation of the C1s signal is due to the increased bond lengths of the amines and the thickness increase of the water adsorption layer as previously described. Critically, the amine content is a truer estimation of the original bromination rates and we can therefore claim that rates of 36-52% have been achieved and therefore approach the

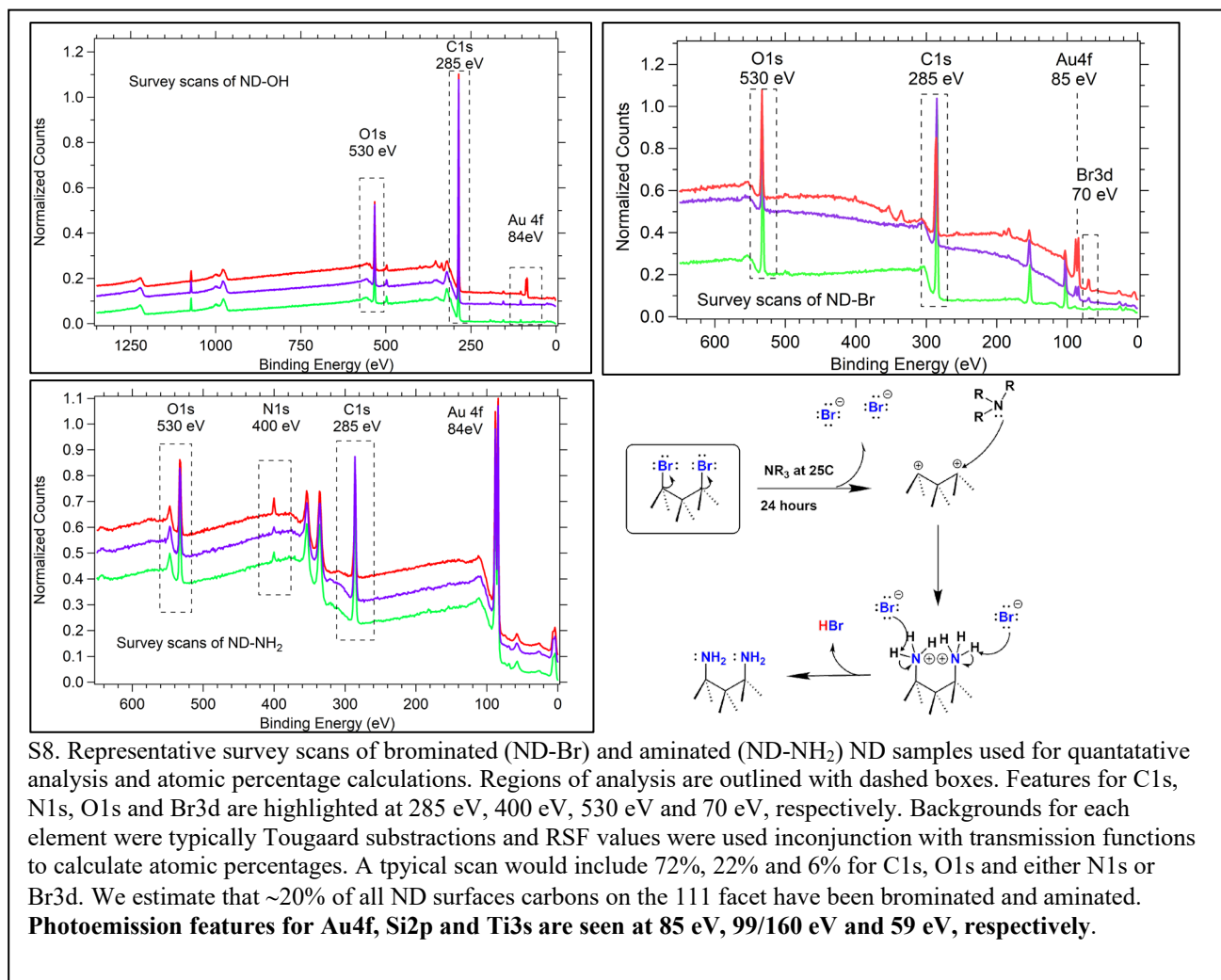


Table S2: Quantitative summary of XPS Survey Scans based on CASAXPS analysis. (10% error assumed for all values).

Sample	Surface Termination	Carbon %	Nitrogen %	Oxygen %	Bromine %
ND-OH-1	Alcohols	86.6	0.0	13.4	0.0
ND-OH-2	Alcohols	85.8	0.0	14.2	0.0
ND-OH-3	Alcohols	87.0	0.0	13.0	0.0
ND-Br-1	Alkyl-bromides	79.4	0.0	20.1	0.5
ND-Br-2	Alkyl-bromides	78.6	0.0	20.3	1.1
ND-Br-3	Alkyl-bromides	73.8	0.0	23.7	2.5
ND-NH ₃ -1	Amines	69.4	7.8	22.8	0.0
ND-NH ₃ -2	Amines	65.5	6.3	28.2	0.0
ND-NH ₃ -3	Amines	69.0	5.4	25.6	0.0

theoretical limits calculated by DFT in Tiwari et al.⁴ Addition of the amines along the ND surface are only possible if preceded by the bromine leaving group, a reactive intermediate being produced and the nucleophilic attack of the surface carbon atom by the approaching NH₃ molecule as illustrated in figure S8. Surface termination of ND constructs after amination chemistry have therefore been quantified to be ~36-52% or 6.5-9.5 atoms of the surface carbon sites. This estimation is based on a predominant {111} crystallographic expression with 18.2 atoms/nm² due to the ball milling process of HPHT diamond as previously discussed.³¹

4E. Low bromine versus higher nitrogen surface species.

The discrepancy between atomic % of Br3d and N1s and the champion samples have 2.5% and 7.8% for Br3d and N1s, respectively. We rationalize this observation due to alkyl-bromides spontaneous degradation as a function of time (post synthesis) and the ultra-high vacuum (UHV) conditions used for XPS, thereby decreasing the percentage contribution during analysis. Adsorption of bromides on Si(100) and Ge(100) have been studied with core-level electron spectroscopy and STM and along with DFT calculations of Br on diamond 111 shows large steric hindrance and low adsorption energies for Br.^{22, 32} Notably, surface bromides on diamond are known via DFT to be highly unstable and never examined physically until now. Increases in O1s signal and decreases in C1s signals during the ND-Br and ND-NH₃ transformations are due to the bulkier surface adsorbates (Br radius of ~180pm versus -OH of ~100 pm) suppressing subsurface diamond photoelectrons. Additionally, after amination chemistry, increases in oxygen content arise from increased adsorbed water on the ND-NH₃ surface (see Figure 1B DRIFTS

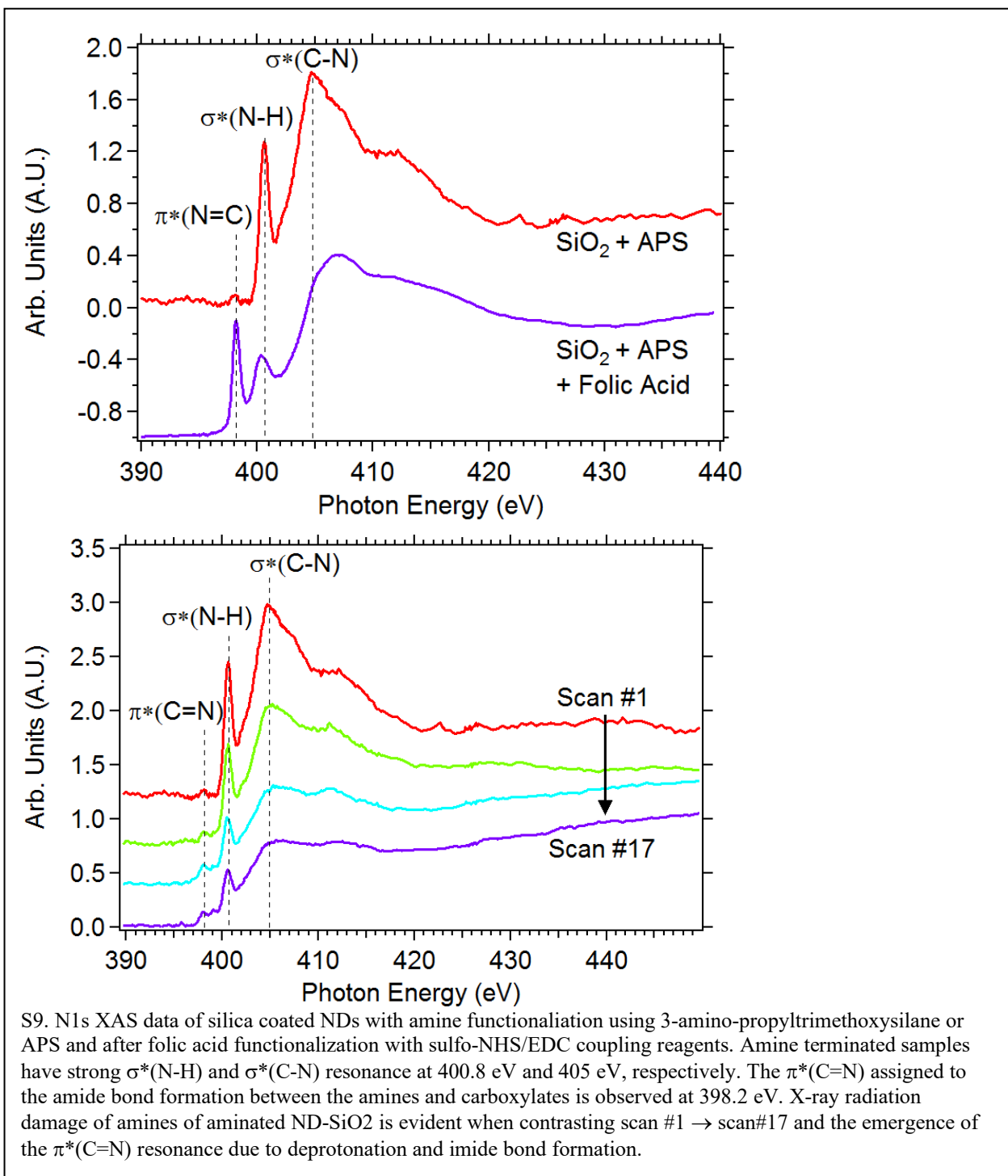
measurement) and would generate a tightly bound water monolayer on the diamond surface that would not desorb at 25°C under UHV conditions.

Table S3: Summary of Surface Groups (-OH, -Br, NH₃ and adsorbed water) based on surface functionalization model. The number in parentheses is the number of surface groups per nm² (atoms/nm²).

Sample	Surface Termination	Alcohol %	Bromide %	Amines %	ML Water
ND-OH-1	Alcohols	89 (16.3)	0.0	0.0	0.0
ND-OH-2	Alcohols	95 (17.3)	0.0	0.0	0.0
ND-OH-3	Alcohols	87 (15.7)	0.0	0.0	0.0
ND-Br-1	Alkyl-bromides	96.7 (17.1)	3.3 (0.6)	0.0	0.0
ND-Br-2	Alkyl-bromides	92.7 (16.1)	7.3 (1.3)	0.0	0.0
ND-Br-3	Alkyl-bromides	83.4 (15.2)	16.6 (3)	0.0	0.0
ND-NH₃-1	Amines	48.0 (8.7)	0.0	52.0 (9.5)	1.0
ND-NH₃-2	Amines	58.0 (10.5)	0.0	42.0 (7.6)	1.0
ND-NH₃-3	Amines	64.0 (11.6)	0.0	36.0 (6.5)	1.0

5. N1s XAS Control Samples, X-ray beam damage and Amide Bond Formation using sulfo-NHS/EDC Coupling.

Conformation of N1s XAS spectra peak positions for $\pi^*(\text{C}=\text{N})$, $\sigma^*(\text{N}-\text{H})$ and $\sigma^*(\text{C}-\text{N})$ was supported by amine functionalization of silica-coated NDs (Figure S9). ND-SiO₂ samples were prepared similar to the route of Cigler et al. and

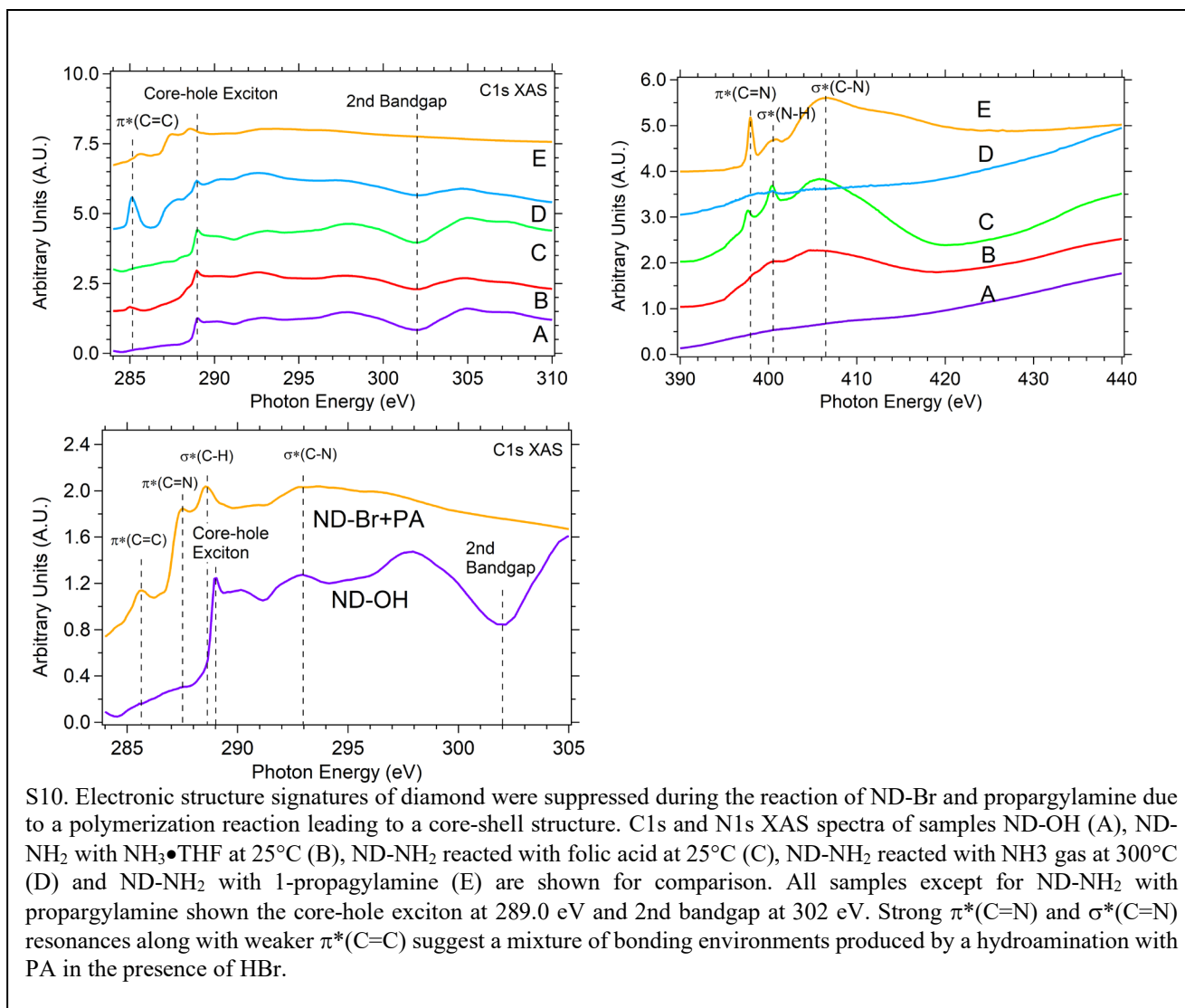


functionalized with 3-amino-propyltrimethoxysilane or APS.³³ Peaks of amine functionalized silica NDs at ~ 400.6 eV and ~ 405.0 eV are assigned to $\sigma^*(\text{N-H})$ and $\sigma^*(\text{N-C})$ resonances, respectively (Figure S9 top). The environment of the N atoms in APS is similar to a single molecule and is bound to the ND-SiO₂ surface through siloxane bonds and is a good model system. The same sample was used for a control conjugation step with amine terminated ND-SiO₂ and folic acid using sulfo-NHS/EDC coupling reagents.³⁴ A new $\pi^*(\text{C=N})$ resonance arise due to the planar amide bond that was formed and is in agreement with the results of ND-NH₂ conjugated to folic acid with sulfo-NHS/EDC coupling (PFY-XAS data in Figure 4C).

We also report the observation of radiation damage of the control ND-SiO₂ samples with amine functionalization and can justify why $\pi^*(\text{C=N})$ resonances may arise in ND-NH₂ samples after X-ray irradiation. In the bottom panel of S9 the emergence of $\pi^*(\text{C=N})$ resonances at 398.2 eV appears after scan #5 and maximizes at scan #17. There is no $\pi^*(\text{C=N})$ resonance at scan #1 and is consistent with a purely C-N and N-H bonding environment around the nitrogen atoms. The impinging X-ray is deprotonating the amine groups (-NH₃) generating an imine bond and the resultant rise of the $\pi^*(\text{C=N})$ bond resonance. X-ray beam damage is common and has been highlighted elsewhere.³⁵

6. Suppression of the diamond electronic structure after propargylamine treatment yields a Sonogashira-type reaction.

N1s and C1s XAS spectra provides surface termination and electronic structure information of the ND constructs and provides evidence of a polymerization reaction with ND-Br and propargylamine (PA). The rationalization for choosing PA as a nucleophile is that PA would render C-N bonds at the diamond surface (assuming nucleophilic attack by the nitrogen center on the carbocation) and retention of the alkyne that would be later used in click-chemistry reactions with azides.³⁶ ND-OH is our control sample and shows clear signatures of diamond with the diamond core-hole exciton and 2nd bandgap at 289.0 eV and 302.0 eV, respectively.¹² ND constructs that



were aerobically oxidized ND-OH (A) and all chemically treated samples with $\text{NH}_3(\text{l}) \bullet \text{THF}$ and $\text{NH}_3(\text{g})$ at 300°C (samples B→D) show clear signatures of diamond's electronic structure, but is not observed in the PA reacted samples (sample E in Figure S10). The PA treated sample was thoroughly purified using DCM and water via centrifugation and decanting cycles. The C1s and N1s spectra of PA treated NDs is therefore representative of the polymerized PA with $\pi^*(\text{C}=\text{N})$, $\pi^*(\text{C}=\text{C})$, $\sigma^*(\text{C}-\text{N})$, $\sigma^*(\text{C}-\text{H})$ and $\sigma^*(\text{N}-\text{H})$ resonances and not the nanodiamond core electronic structure. Control reactions of ND-Br with N-Boc propargylamine did not show strong nitrogen signals, did not suppress the diamond electronic structure and suggests that the polymerization pathway was sterically halted by the N-Boc protecting group on the nitrogen center (data not shown).

Suppression of a substrate electronic structure information has been previously reported for SiO_2 on Si substrates and SiO_2 on highly ordered pyrolytic graphite using total electron yield (TEY) and fluorescence yield (FY) measurements.³⁷⁻³⁸ TEY measurements from Kasrai et al. found a probe depth of 5 nm for the L-edge and 70 nm for the K-edge of Si. Our XAS measurements in TEY mode for C1s probe 5-10 nm into a sample and complete suppression of the diamond electronic structure suggests we have a minimum of 5 nm of a PA-based shell on our ND core.

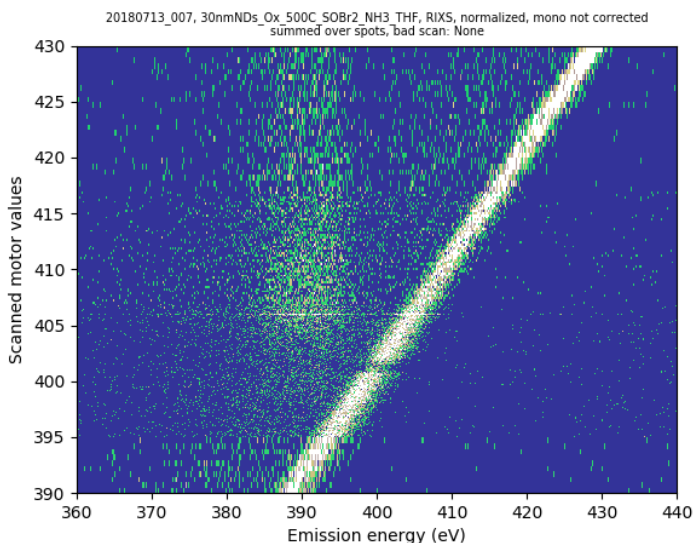
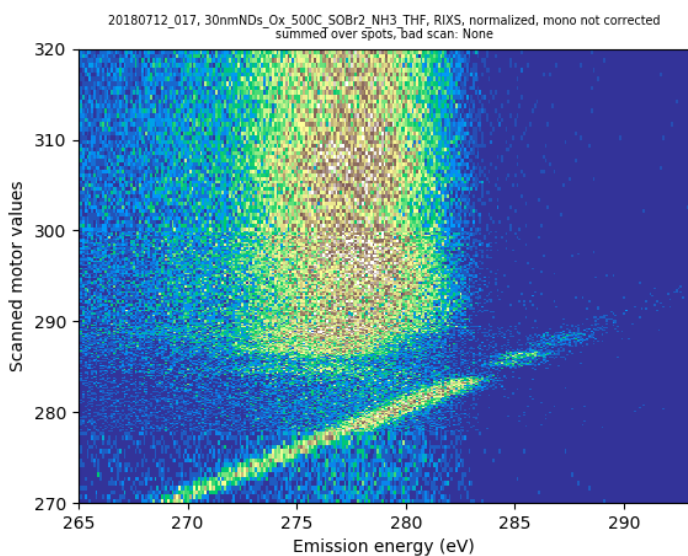
The detailed mechanism for the polymerization is unknown and beyond the scope of this paper and could be initiated through the carbocation on the diamond surface, the high reactivity of propargylamine and the presence of Br^- in solution. Either the amine or alkyne portion of the propargylamine could react with the carbocation surface after the dissociation of the bromide ion. The reaction could be summarized as a hydroamination or Sonogarisha-type reaction. One possible mechanism is speculated whereby the amine performs the initial nucleophilic attack on the carbocation, a deprotonation occurs on the nitrogen center and then the outward facing alkyne is reacted with the amine of a free PA precursor in solution. A second route could be a carbocation polymerization with the alkyne adding across the carbocation. Carbocation polymerizations are common yet not previously demonstrated through the use of a brominated diamond substrate.³⁹ Mechanistic details can be elucidated through screening a library of alkynes and altering the concentration of the nucleophilic species and will be further studied. The termination of the reaction was at the 24-hour mark when the stirred solution at 25°C was purified multiple times

through centrifugation and decantation cycles. A mechanism for polyimine formation will be generated after these additional experiments are conducted.

7. Representative Carbon, Nitrogen and Oxygen RIXS Maps of aminated ND-Br samples

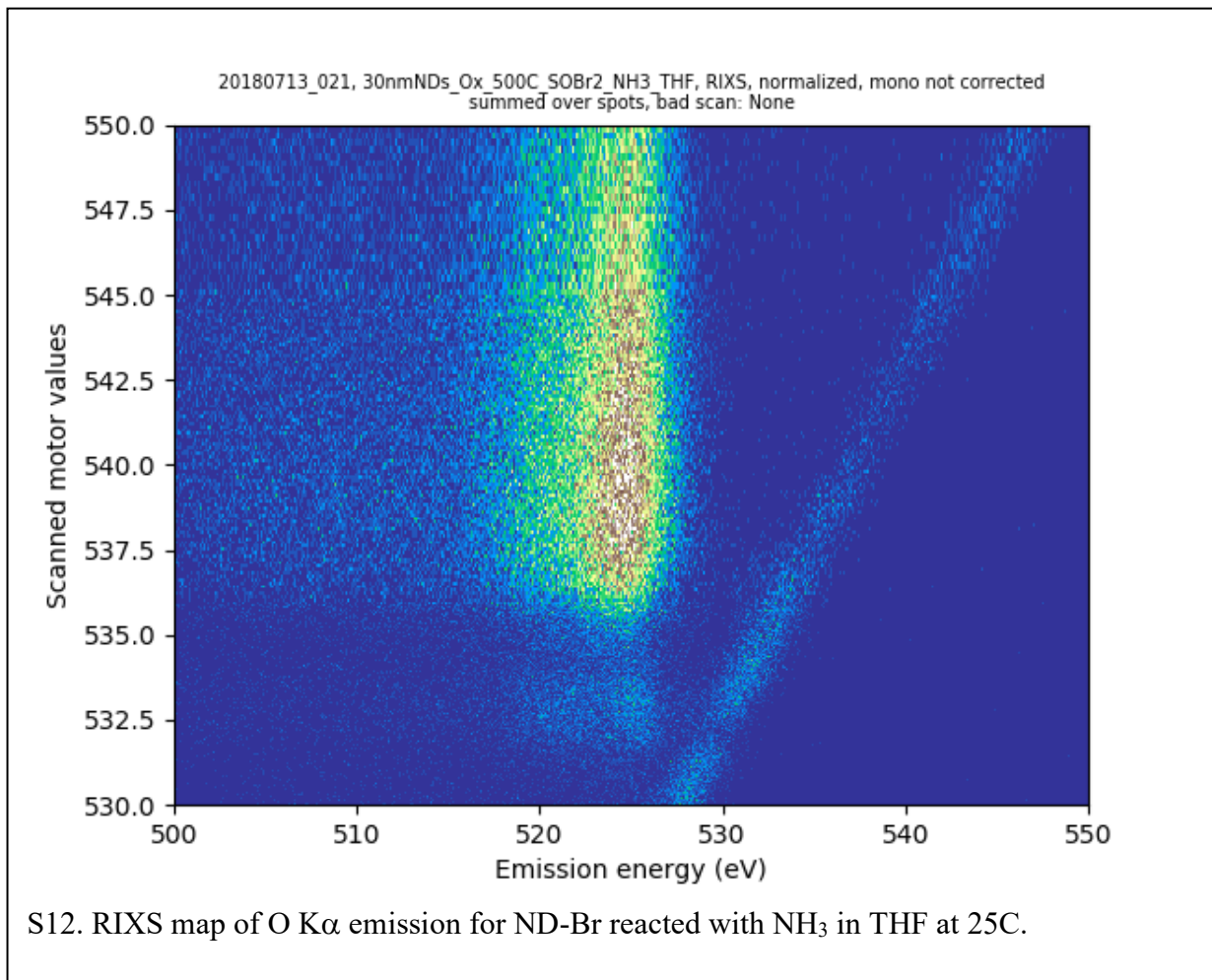
The RIXS maps below are the raw data sets from the line integrations presented in figure 4A within the manuscript. Samples were prepared in 3 motifs with the $\text{NH}_3 \bullet \text{THF}$ route at 25°C , in neat liquid NH_3 at -77°C and at elevated temperatures in the presence of NH_3 gas in a tube furnace. Data presented in Figure 4A where integrated counts within an excitation photon energy range (y-axis) and plotted against the X-ray emission photon energies (x-axis). Please see the

7A. ND-Br reacted with NH_3 in THF at 25°C RIXS Maps

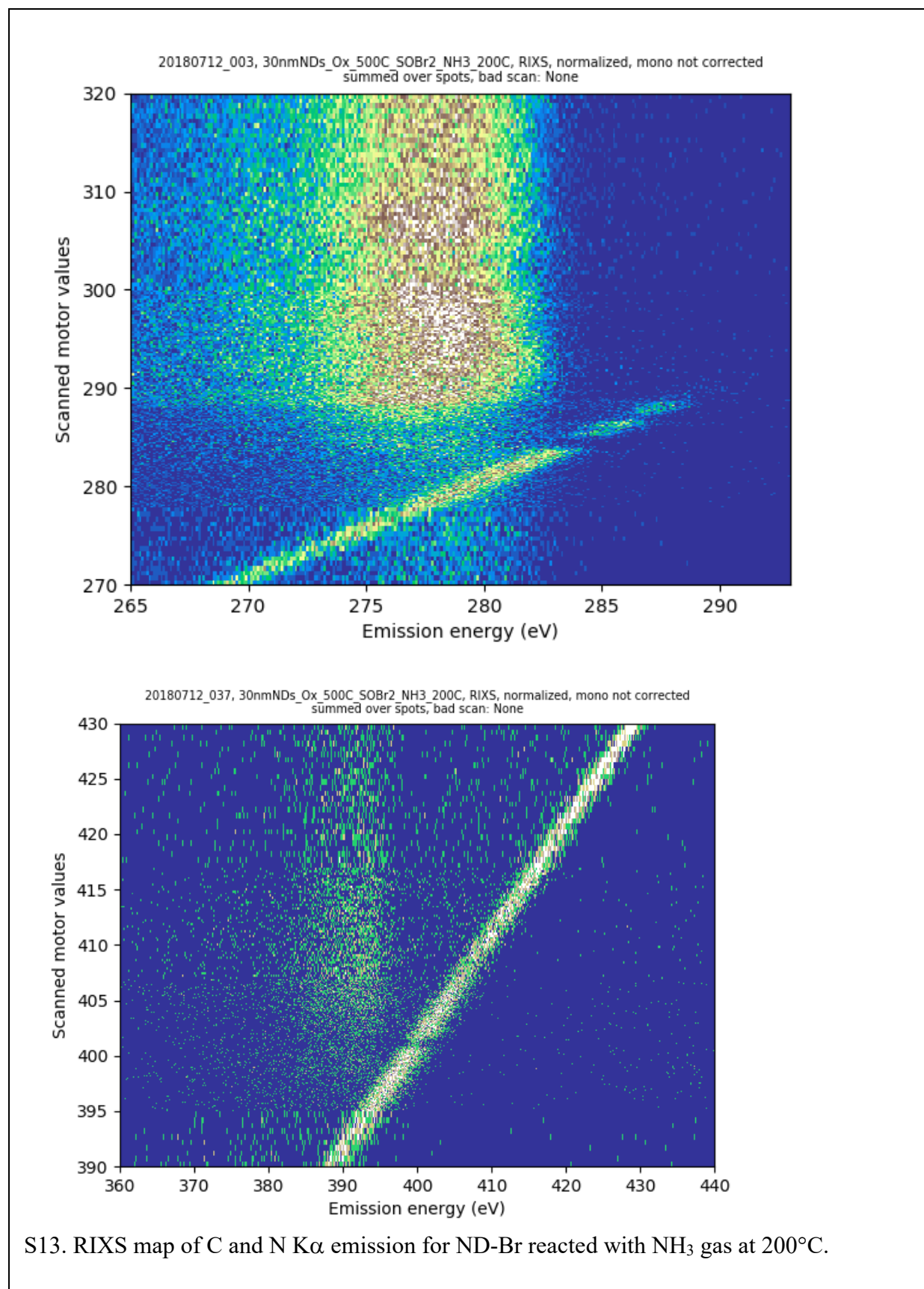


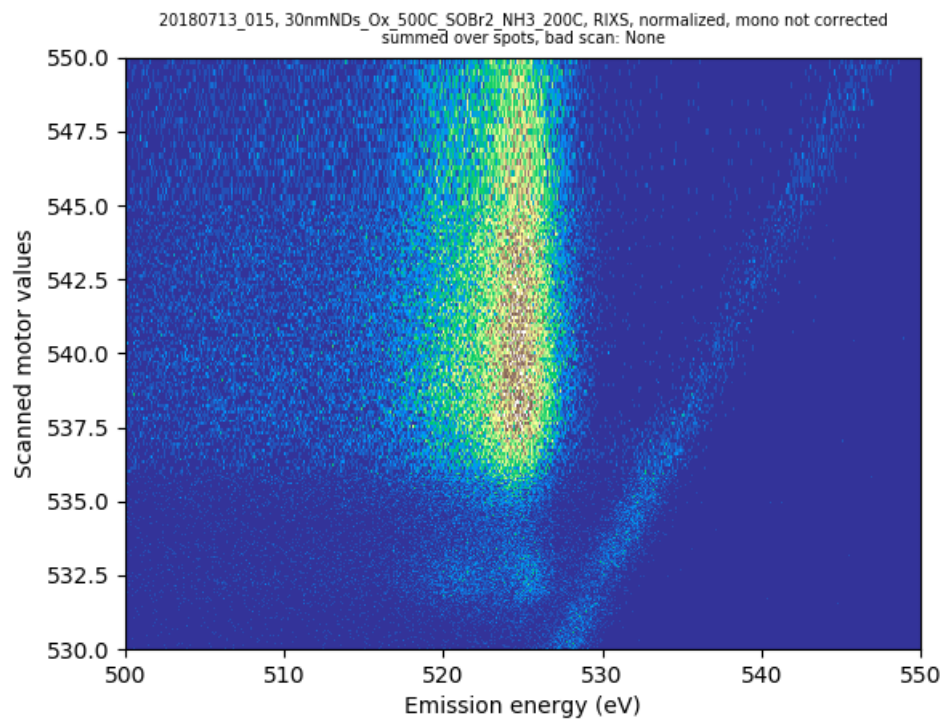
S11. RIXS map of C and N $\text{K}\alpha$ emission for ND-Br reacted with NH_3 in THF at 25°C .

manuscript for a summary and conclusions of the RIXS data collected with the TES detector at beamline 10-1 at SSRL. The sample description is given in bold at the top of the raw data sets.



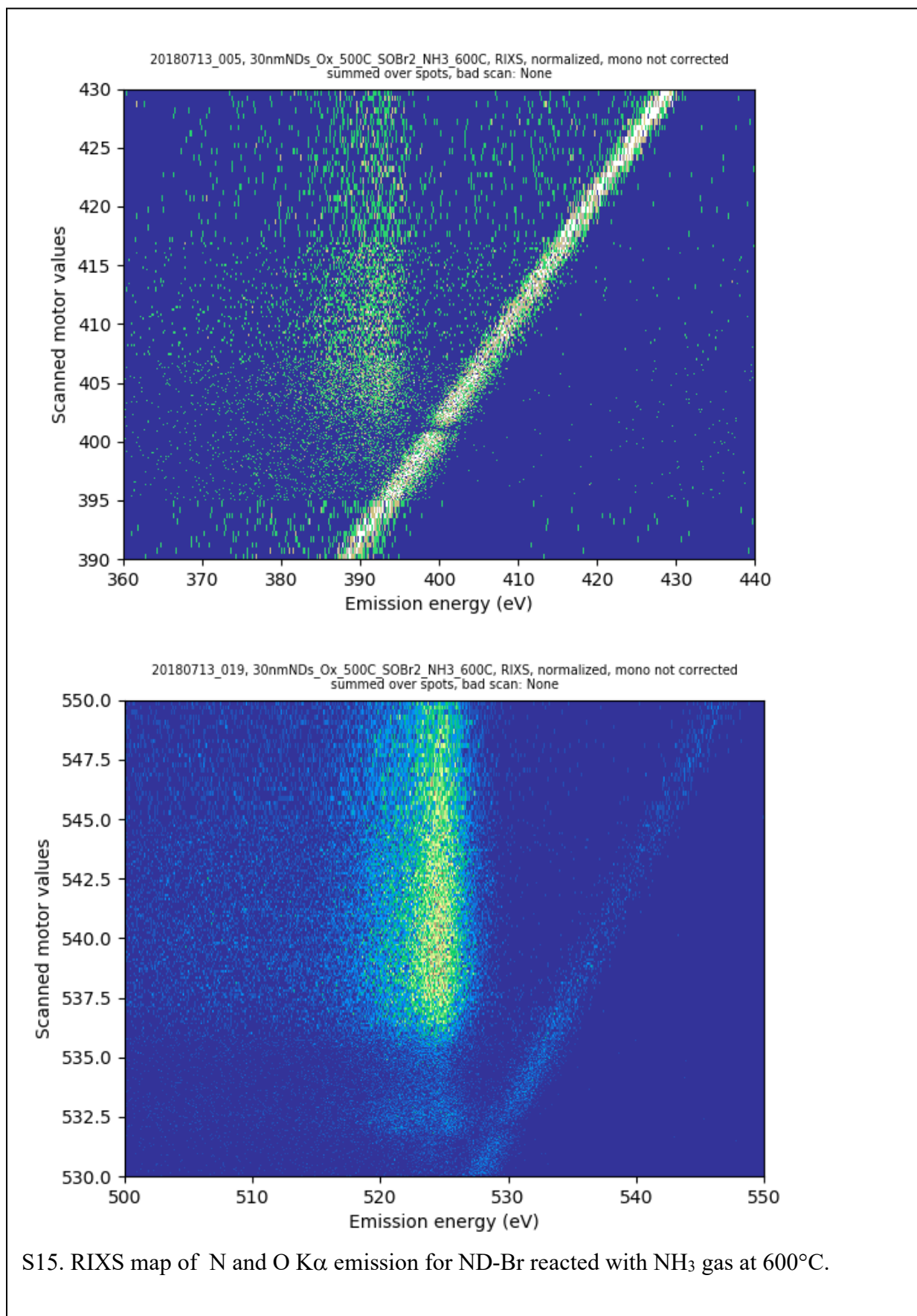
7B. ND-Br reacted with NH₃ gas at 200°C RIXS Maps





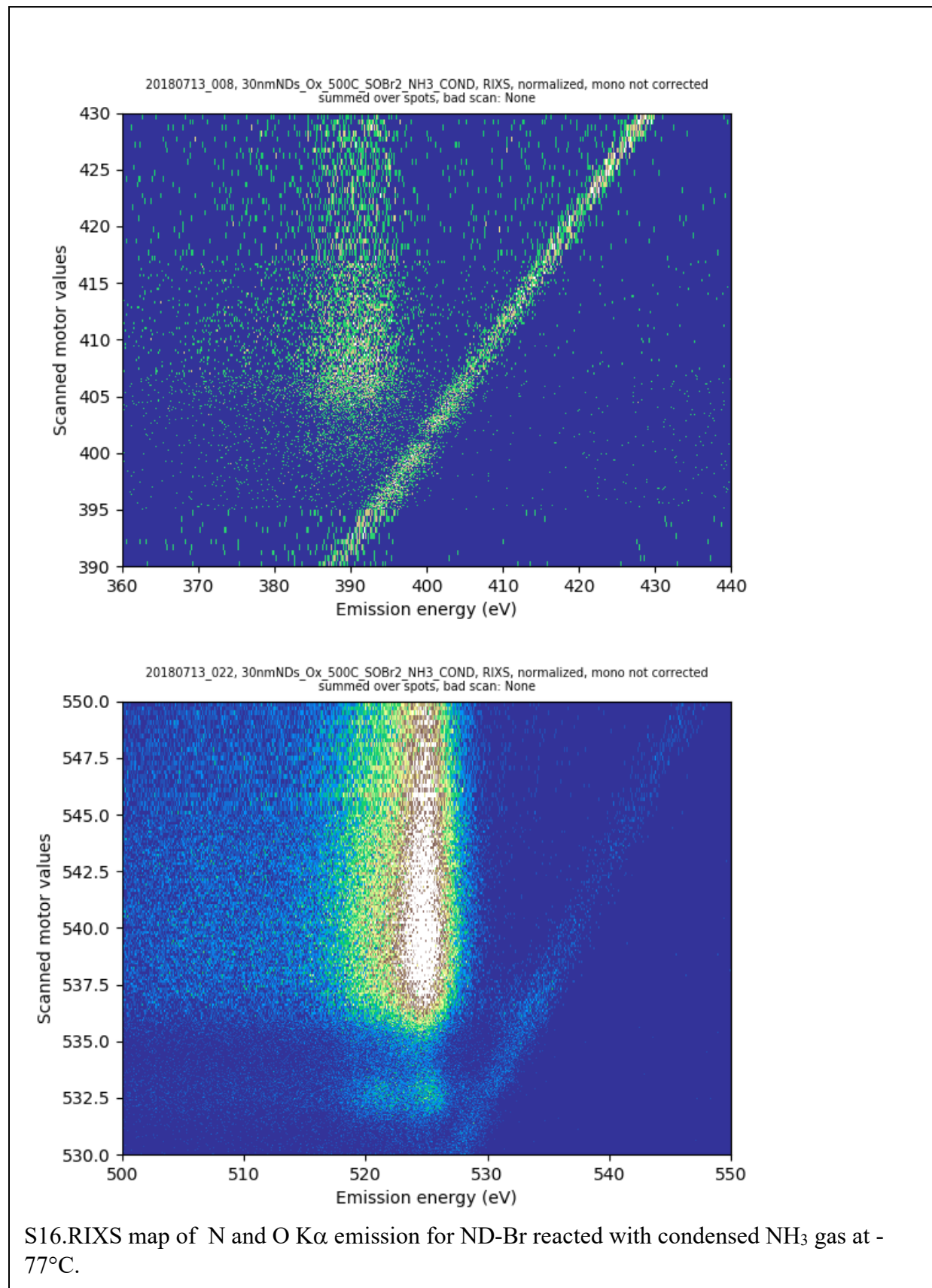
S14. RIXS map of O $K\alpha$ emission for ND-Br reacted with NH_3 gas at 200°C .

7C. ND-Br reacted with NH₃ gas at 600°C RIXS Maps



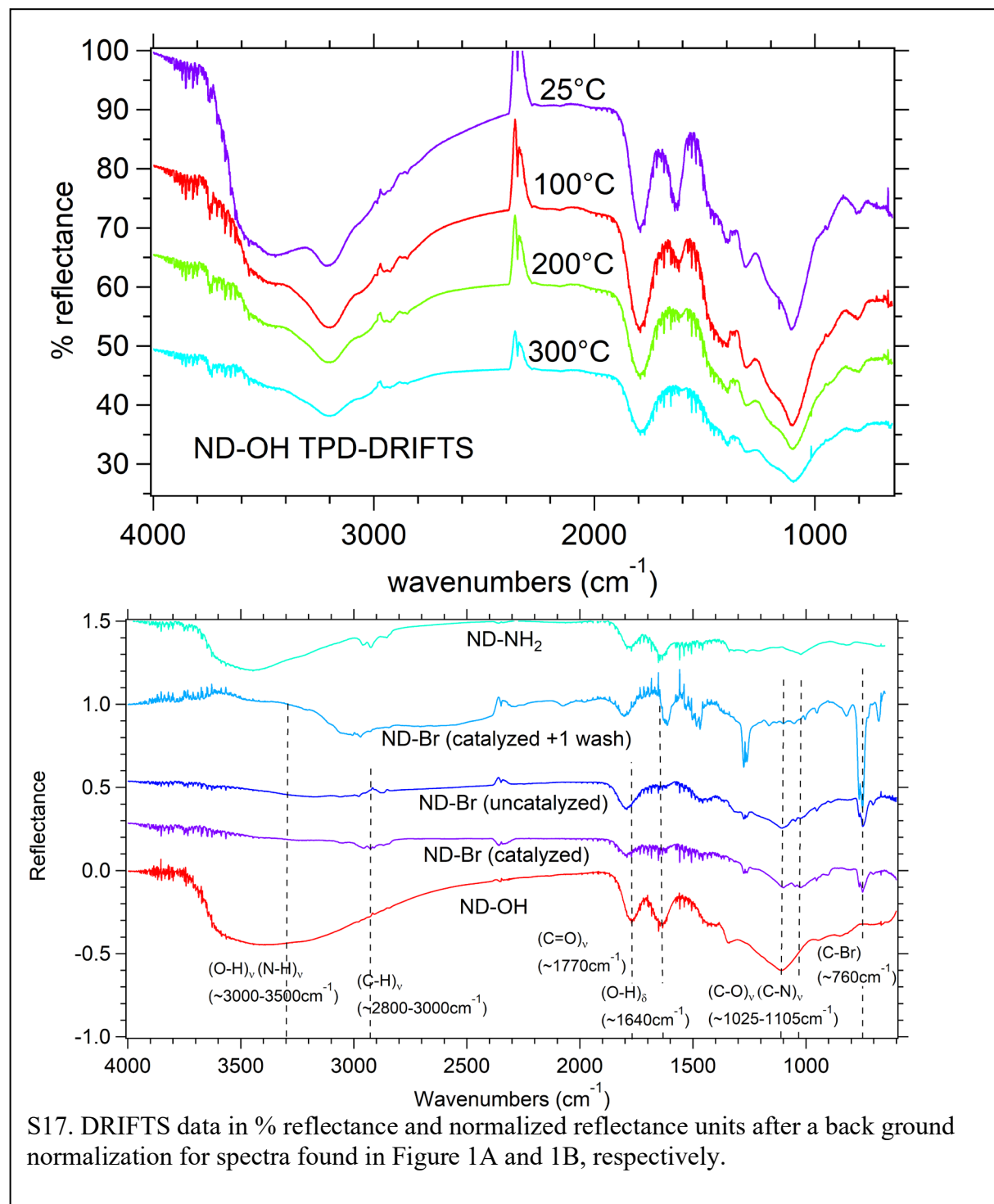
7D. ND-Br reacted with condensed NH₃ at -77°C

References

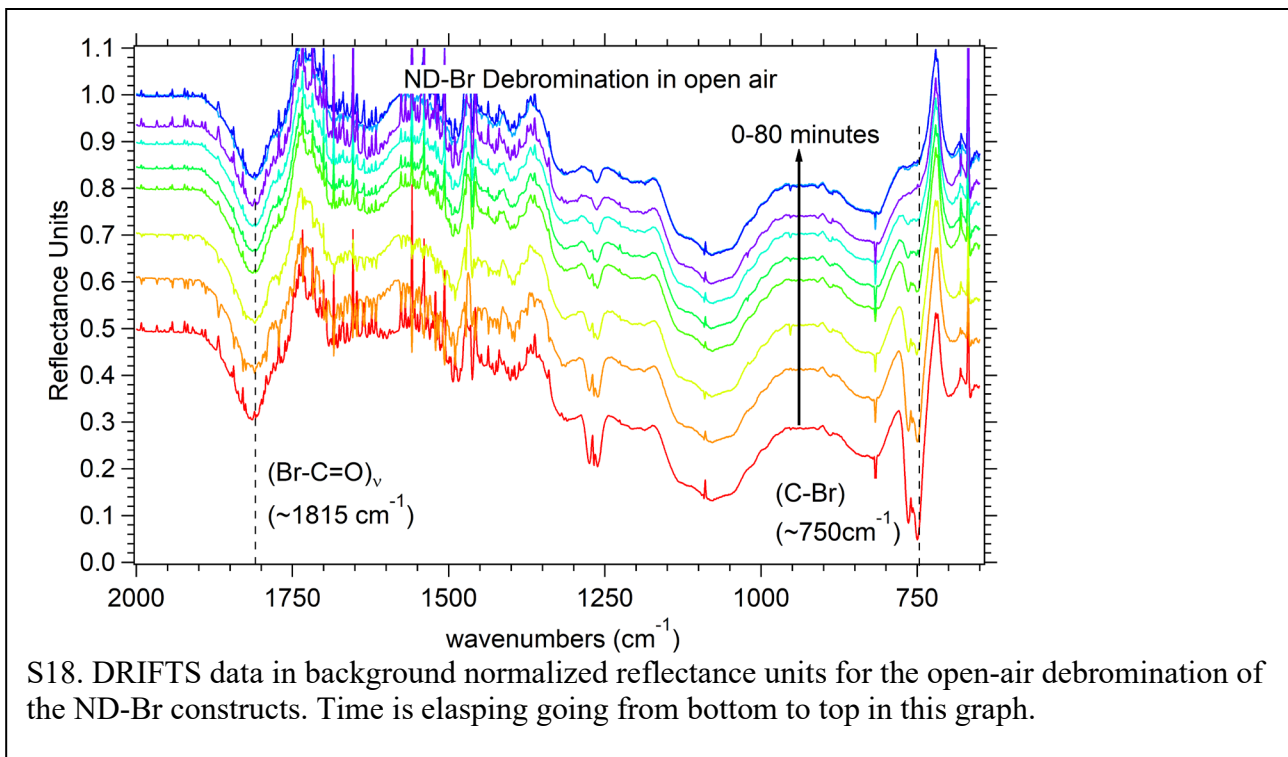


8. Percent Reflectance and Normalized Reflectance Spectra of TPD-DRIFTS, and other DRIFTS spectra from Figure 1

This spectra represents the raw data taken in % reflectance units for the TPD-DRIFTS study of oxidized HPHT NDs from 25→300°C in open air conditions and watching the (O-H)_v and (O-H)_δ decrease as a function of temperature. Other



S17. DRIFTS data in % reflectance and normalized reflectance units after a back ground normalization for spectra found in Figure 1A and 1B, respectively.



References

1. Seah, M. P.; Dench, W. A., Quantitative Electron Spectroscopy of Surfaces: A Standard Data Base for Electron Inelastic Mean Free Paths in Solids. *Surface and Interface Analysis* **1979**, *1*, 2-11.
2. Miyamoto, Y.; Saito, M., Electron Injection into Conduction Bands of the Diamond (100) Surface by Nitrogen Impurities. *Physical Review B* **1998**, *57*, 6527-6533.
3. Loh, K. P.; Xie, X. N.; Yang, S. W.; Zheng, J. C., Oxygen Adsorption on (111)-Oriented Diamond: A Study with Ultraviolet Photoelectron Spectroscopy, Temperature-Programmed Desorption, and Periodic Density Functional Theory. *Journal of Physical Chemistry B* **2002**, *106*, 5230-5240.
4. Tiwari, A. K.; Goss, J. P.; Briddon, P. R.; Wright, N. G.; Horsfall, A. B.; Rayson, M. J., Bromine Functionalisation of Diamond: An Ab Initio Study. *Physica Status Solidi a-Applications and Materials Science* **2012**, *209*, 1703-1708.
5. Miller, J. B., Order, Disorder, and Quasioder in the Hydrogen-Bond Networks of Diamond-Nh₂ Surfaces. *Journal of Chemical Physics* **2001**, *115*, 2303-2311.
6. CasaXPS, *Casaxps User's Manual*, 2001, p 163.
7. Socrates, G., *Infrared and Raman Characteristic Group Frequencies: Tables and Charts*, 3rd ed.; John Wiley and Sons: London, 2001, p 343.
8. Osswald, S.; Yushin, G.; Mochalin, V.; Kucheyev, S. O.; Gogotsi, Y., Control of Sp(2)/Sp(3) Carbon Ratio and Surface Chemistry of Nanodiamond Powders by Selective Oxidation in Air. *Journal of the American Chemical Society* **2006**, *128*, 11635-11642.
9. Krueger, A.; Lang, D., Functionality Is Key: Recent Progress in the Surface Modification of Nanodiamond. *Advanced Functional Materials* **2012**, *22*, 890-906.
10. Krueger, A.; Stegk, J.; Liang, Y.; Lu, L.; Jarre, G., Biotinylated Nanodiamond: Simple and Efficient Functionalization of Detonation Diamond. *Langmuir* **2008**, *24*, 4200-4204.
11. Girard, H. A.; Petit, T.; Perruchas, S.; Gacoin, T.; Gesset, C.; Arnault, J. C.; Bergonzo, P., Surface Properties of Hydrogenated Nanodiamonds: A Chemical Investigation. *Physical Chemistry Chemical Physics* **2011**, *13*, 11517-11523.
12. Morar, J. F.; Himpsel, F. J.; Hollinger, G.; Hughes, G.; Jordan, J. L., Observation of a C-1s Core Exciton in Diamond. *Physical Review Letters* **1985**, *54*, 1960-1963.
13. Lee, S. J., et al., Soft X-Ray Spectroscopy with Transition-Edge Sensors at Stanford Synchrotron Radiation Lightsource Beamline 10-1. *Review of Scientific Instruments* **2019**, *90*.
14. Lee, S. J.; Mori, R.; Alpert, B.; Baker, M.; Berry, J.; Cho, H.-M.; Denison, E.; Doriese, W.; Fowler, J.; Gaffney, K. In *Ultrasensitive Probing of the Local Electronic Structure of Nitrogen Doped Carbon and Its Applications to 2d Electronics, Catalysis and Bio-Physics*, ABSTRACTS OF PAPERS OF THE AMERICAN CHEMICAL SOCIETY, AMER CHEMICAL SOC 1155 16TH ST, NW, WASHINGTON, DC 20036 USA: 2017.
15. Saikia, I.; Borah, A. J.; Phukan, P., Use of Bromine and Bromo-Organic Compounds in Organic Synthesis. *Chemical Reviews* **2016**, *116*, 6837-7042.
16. Djerassi, C.; Scholz, C. R., Brominations with Pyridine Hydrobromide Perbromide. *Journal of the American Chemical Society* **1948**, *70*, 417-418.
17. Williamson, A., Xlv. Theory of Ætherification. *The London, Edinburgh, and Dublin Philosophical Magazine and Journal of Science* **1850**, *37*, 350-356.
18. Johnstone, R. A. W.; Rose, M. E., Rapid, Simple, and Mild Procedure for Alkylation of Phenols, Alcohols, Amides and Acids. *Tetrahedron* **1979**, *35*, 2169-2173.

19. Regen, S. L.; Besse, J. J.; McLick, J., Solid-Phase Cosolvents - Triphase Catalytic Hydrolysis of 1-Bromoadamantane. *Journal of the American Chemical Society* **1979**, *101*, 116-120.
20. Olah, G. A.; Reddy, V. P.; Prakash, G. K. S., Long-Lived Cyclopropylcarbinyl Cations. *Chemical Reviews* **1992**, *92*, 69-95.
21. Olah, G. A.; Liang, G.; Babiak, K. A.; Ford, T. M.; Goff, D. L.; Morgan, T. K.; Murray, R. K., Structure of Cyclopropylcarbinyl and Cyclobutyl Cations - 8,9-Dehydro-2-Adamantyl and 2,5-Dehydro-4-Protoadamantyl Cations. *Journal of the American Chemical Society* **1978**, *100*, 1494-1500.
22. Larsson, K.; Lunell, S., Stability of Halogen-Terminated Diamond (111) Surfaces. *Journal of Physical Chemistry A* **1997**, *101*, 76-82.
23. Luo, Y.-R., *Comprehensive Handbook of Chemical Bond Energies*; Taylor & Francis Group: Baton Rouge, UNITED STATES, 2007.
24. Freedman, A., Halogenation of Diamond (100) and (111) Surfaces by Atomic-Beams. *Journal of Applied Physics* **1994**, *75*, 3112-3120.
25. Kazakbayeva, Z.; Zhmagali, S.; Mahboob, A.; O'Reilly, R. J., Homolytic C-Br Bond Dissociation Energies Obtained by Means of the G4 Thermochemical Protocol. *Chemical Data Collections* **2016**, *2*, 43-48.
26. Seah, M. P., Simple Universal Curve for the Energy-Dependent Electron Attenuation Length for All Materials. *Surface and Interface Analysis* **2012**, *44*, 1353-1359.
27. Seah, M. P., An Accurate and Simple Universal Curve for the Energy-Dependent Electron Inelastic Mean Free Path. *Surface and Interface Analysis* **2012**, *44*, 497-503.
28. de Theije, F. K.; Reedijk, M. F.; Arsic, J.; van Enckevort, W. J. P.; Vlieg, E., Atomic Structure of Diamond {111} Surfaces Etched in Oxygen Water Vapor. *Physical Review B* **2001**, *64*, 085403.
29. Wang, X. F.; Ruslinda, A. R.; Ishiyama, Y.; Ishii, Y.; Kawarada, H., Higher Coverage of Carboxylic Acid Groups on Oxidized Single Crystal Diamond (001). *Diamond and Related Materials* **2011**, *20*, 1319-1324.
30. Kono, S., et al., Carbon 1s X-Ray Photoelectron Spectra of Realistic Samples of Hydrogen-Terminated and Oxygen-Terminated Cvd Diamond (111) and (001). *Diamond and Related Materials* **2019**, *93*, 105-130.
31. Wolcott, A.; Schiros, T.; Trusheim, M. E.; Chen, E. H.; Nordlund, D.; Diaz, R. E.; Gaathon, O.; Englund, D.; Owen, J. S., Surface Structure of Aerobically Oxidized Diamond Nanocrystals. *Journal of Physical Chemistry C* **2014**, *118*, 26695-26702.
32. Hou, H. Y.; Wu, H. H.; Chung, J. Y.; Lin, D. S., Adsorption of Diatomic Interhalogens on the Si(100) and Ge(100) Surfaces. *Journal of Physical Chemistry C* **2011**, *115*, 13262-13267.
33. Rehor, I., et al., Plasmonic Nanodiamonds: Targeted Core-Shell Type Nanoparticles for Cancer Cell Thermoablation. *Advanced Healthcare Materials* **2015**, *4*, 460-468.
34. Hermanson, G. T., *Bioconjugate Techniques*, 2nd Edition ed.; Elsevier, 1996, p 1202.
35. Leinweber, P.; Kruse, J.; Walley, F. L.; Gillespie, A.; Eckhardt, K.-U.; Blyth, R. I. R.; Regier, T., Nitrogen K-Edge Xanes - an Overview of Reference Compounds Used to Identify 'Unknown' Organic Nitrogen in Environmental Samples. *Journal of Synchrotron Radiation* **2007**, *14*, 500-511.
36. Nandivada, H.; Jiang, X.; Lahann, J., Click Chemistry: Versatility and Control in the Hands of Materials Scientists. *Advanced Materials* **2007**, *19*, 2197-2208.

37. Kasrai, M.; Lennard, W. N.; Brunner, R. W.; Bancroft, G. M.; Bardwell, J. A.; Tan, K. H., Sampling Depth of Total Electron and Fluorescence Measurements in Si L- and K-Edge Absorption Spectroscopy. *Applied Surface Science* **1996**, *99*, 303-312.
38. Baba, Y.; Shimoyama, I.; Hirao, N.; Sekiguchi, T., Structure of Ultra-Thin Silicon Film on HOPG Studied by Polarization-Dependence of X-Ray Absorption Fine Structure. *Chemical Physics Letters* **2014**, *594*, 64-68.
39. Goethals, E. J.; Du Prez, F., Carbocationic Polymerizations. *Progress in Polymer Science* **2007**, *32*, 220-246.